Ankyrin-B: proteostasis and impact on cardiomyocyte behaviours in H9c2 cells

by

Lena Chen
B.Sc., University of Ottawa, 2015

A Thesis Submitted in Partial Fulfillment
of the Requirements for the Degree of

Master of Science

in the Division of Medical Sciences

Supervisory Committee

Ankyrin-B: proteostasis and impact on cardiomyocyte behaviours in H9c2 cells

by

Lena Chen
B.Sc., University of Ottawa, 2015

Supervisory Committee

Dr. Leigh Anne Swayne, Division of Medical Sciences
Supervisor

Dr. Laura Arbour, Division of Medical Sciences
Co-Supervisor

Dr. Raad Nashmi, Department of Biology
Outside Member

Dr. Chris Nelson, Department of Biochemistry and Microbiology
Outside Member

Abstract

Supervisory Committee
Dr. Leigh Anne Swayne, Division of Medical Sciences
Supervisor
Dr. Laura Arbour, Division of Medical Sciences
Co-Supervisor
Dr. Raad Nashmi, Department of Biology
Outside Member
Dr. Chris Nelson, Department of Biochemistry and Microbiology
Outside Member

Ankyrin-B (Ank-B) is a crucial scaffolding protein regulating expression and localization of contractile machinery in the cardiac muscle. Recent genetic investigations in the First Nations Community, the Gitxsan of Northern BC, identified a mutation in Ank-B (p.S646F c.1937 C>T) associated with a cardiac arrhythmia, Long QT Syndrome Type 4 (LQTS4). Distinct from other LQTS4 subtypes, individuals harbouring the p.S646F variant exhibit development deficits including cardiomyopathies and accessory electrical pathways. How p.S646F interferes with the development of the heart is unknown due to a fundamental lack of understanding regarding Ank-B proteostasis and its role in cardiac differentiation. Initial *in silico* analyses predicted the p.S646F mutant to be deleterious to the Ank-B protein. Using *in vitro* techniques, I determined p.S646F mutant reduced levels of Ank-B in H9c2 rat ventricular cardiomyoblasts. Furthermore, haploinsufficiency in mice was previously shown to result in developmental cardiac deficits. I, therefore, hypothesized that p.S646F interferes with Ank-B proteostasis, thereby affecting cardiomyocyte development. I showed that p.S646F destabilized Ank-B in cardiomyoblasts, due to increased degradation via the proteasome. Furthermore, overexpression of p.S646F Ank-B had a significant impact on cellular behaviour including reduced cell viability, and altered expression of cellular differentiation markers. Together these data address critical knowledge gaps with regards to Ank-B protein homeostasis and the role of Ank-B in cardiomyocyte viability and development. These findings inform the diagnosis and treatment of patients with the p.S646F variant, creating potential targeted pathways of intervention, and furthering our understanding of the role of the Ank-B in the development of the heart.

Publications

Original Research:

1. Swayne LA, Murphy P, Asuri S, Chen L, Xu X, McIntosh S, Wang C, Lancione PJ, Roberts JD, Kerr C, Sanatai S, Sherwin E, Klin CF, Zhang M, Mohler P, Arbour LT. Novel variant in the *ANK2* membrane-binding domain is associated with Ankyrin-B Syndrome and structural heart disease in a First Nations population with a high rate of LongQT Syndrome. *Circulation: Cardiovascular Genetics.*10(1) doi:10.1161/CIRCGENETICS.116.001537.

Conference Presentation Abstracts:

1. Chen L, Arbour L, Swayne LA. Turnover of the Ankyrin-B scaffold protein is regulated by the proteasome and affects cardiomyocyte development. (Canadian Society for Molecular Biology Annual Meeting 2017, poster presentation by L Chen)

2. Chen L, Murphy N, McIntosh S, Asuri S, Kerr C, Sanatani S, Sherwin E, Mohler P, Swayne LA, Arbour L. Novel mutation in *ANK2* membrane-binding domain is associated with Ankyrin-B syndrome & structural heart disease in First Nations community of Northern British Columbia. (American Society for Human Genetics Annual Meeting 2016, poster presentation by L Chen)

Table of Contents

List of Figures

List of Abbreviations

4-PBA – 4-phenylbutyrate

AKAP – A-Kinase anchoring protein

Ank – ankyrin protein

ANK1 – gene encoding ankyrin-R

ANK2 – gene encoding ankyrin-B

ANK3 – gene encoding ankyrin-G

Ank-B – ankyrin-B protein

Ank-B syndrome – Ankyrin-B Syndrome

Ank-G – ankyrin-G protein

Ank-R – ankyrin-R protein

ANOVA – analysis of variance

ATCC – American Type Culture Collection

ATF6 – activating transcription factor 6

ATF4 – activating transcription factor 4

ATPase – adenosine tri-phosphate hydrolase

BafA – bafilomycin A

Bcl-2- B-cell lymphoma 2

BiP – binding immunoglobulin protein

BIN2 – bridging integrator 1

Ca^{2+} – calcium

$Ca_v1.2$ – L-type calcium channel, α1C pore forming subunit

$Ca_v1.3$ – L-type calcium channel, α1D pore forming subunit

CD – circular dichromism

CHX – cycloheximide, eukaryotic protein synthesis inhibitor

Cx43 – connexin 43

cTnT – cardiac troponin T

DDT – diothiothreitol

DMEM – Dulbecco's modified Eagle medium

DMSO – dimethylsulfoxide

ECG – electrocardiogram

EDTA – ethylenediaminetetraacetic acid

ER – endoplasmic reticulum

ERAD – endoplasmic reticulum associated degradation

FBS – fetal bovine serum

FPLC – fast protein liquid chromatography

GFP – green fluorescent protein

H9c2 – *Rattus norvegicus* ventricular-derived embryonic cardiomyoblast cell line

HEK293T – *Homo sapiens* embryonic kidney cell line

Hl-1 – *Mus musculus* atrial-derived cardiomyocyte cell line

HRP – horseradish peroxidase

Hsp – heat shock protein or chaperone protein

IgG – Immunoglobulin G

IRE1 – inositol requiring protein 1a

K^+ – potassium

KCl – potassium chloride

kDa – kilodalton

LQTS – long QT syndrome

LQTS4 – long QT syndrome type 4

MBD – membrane binding domain of ankyrin-B

MHC – myosin heavy chain

MTT – 3-(4,5-Dimethylthiazol-2-yl)-2,5-diphenyltetrazolium bromide, cell viability dye

Na^+ – sodium

NCX1 – Na^+ Ca^{2+} exchanger

NKA – Na^+ K^+ ATPase

PBS – phosphate buffered saline

PBS-T – phosphate buffered saline with 0.1% Tween-20

PCR – polymeraise chain reaction

PDL – poly-D-lysine

PERK – protein kinase RNA-like ER kinase

PFA – paraformaldehyde

PI – propidium iodide, fluorescent DNA-intercalating stain evaluates cell viability

PMSF – phenylmethylsufonyl fluoride

PQC – protein quality control

PS-341 – bortezomib, selective proteasome inhibitor

PSD-95 – Post synaptic density protein 95

PVDF – polyvinyl fluoride

QTc – corrected QT interval, QT interval corrected for heart rate as measured by ECG

RA – ATRA – all-*trans*-retinoic acid

RD – regulatory domain of Ankyirn-B

RIPA– radioimmunoprecipitation assay, cell lysis and protein extraction buffer

rpm – rotations per minute

RT-PCR – real-time polymerase chain reaction

SBD – spectirn binding domain of ankyrin-B

SDS – sodium dodecyl sulfate

p.S646F – serine substitution for phenylalanine at amino acid 646 of the ankyrin-B protein

SAN – sinoatrial node

SDS-PAGE – sodium dodecyl sulphate polyacrylamide gel electrophoresis

SR – sarcoplasmic reticulum

TAPVR – total anomalous pulmonary vein return

TCA Cycle – tricarboxylic acid cycle

T-tubule – transverse tubule

UPR – unfolded protein response

UPS – Ubiquitin-Protease System

WPW – Wolff-Parkinson-White Syndrome

WT – wildtype

Acknowledgments

I owe great thanks to both my supervisors, Dr. Leigh Anne Swayne and Dr. Laura Arbour, for the rewarding experience of contributing to the critical field of basic science with direct translational applications. I am deeply grateful for the support, patience, and guidance of two incredibly dedicated researchers. Thank you, Dr. Leigh Anne Swayne, for embodying overflowing passion and sincere curiosity in all scientific endeavours. I am grateful for the opportunity to have studied under your mentorship, and have learned, by example and through direct leadership, that true grit and perseverance are rewarded with the exhilaration of discovery. I would also like to individually thank Dr. Laura Arbour for providing continuous support throughout the unpredictability of graduate research. Thank you for unwaveringly articulating the patient perspectives and human impact that are the foundation and future of this body of research. I also thank my committee members, Dr. Raad Nashmi and Dr. Chris Nelson, for providing expert advice, constructive criticism, and enthusiasm throughout the duration of my project.

Acknowledgement must be made with respect to the Esquimalt, W̲SÁNEĆ, and Songhees peoples on whose traditional territory the University of Victoria stands and the place in which this research was conducted. Importantly, acknowledgement and sincere gratitude must be extended to the on-going partnership with the Gitxsan Health Society in their research goals and participants.

Funding agencies supporting the work in this thesis were provided by Michael Smith Foundation for Health Research, British Columbia Schizophrenia Society Foundation Scholar, and University of Victoria seed funds awarded to Dr. Swayne. The clinical cohort was funded by the Canadian Institute of Health Research (CIHR) of

Ottawa, Ontario [research grant no. 81197]. Additional funding was awarded to Dr. Arbour and Dr. Swayne by Canadian Institutes of Health Research bridge funding. I was supported by the Natural Sciences and Engineering Research Council Alexander Graham Bell Canadian Graduate Scholarship-Master's, and University of Victoria donor awards.

Thanks to the past and present members of the Swayne Lab, that have supported me throughout the project. Thank you, Leigh Wicki-Stordeur and Andrew Boyce for all the hours spent training. Thanks Catherine Choi and Juan Sanchez-Arias for western blot and imaging contributions. Thanks to those in the lab I spent the earliest mornings and latest evenings with, including Andrew Boyce, Juan Sanchez-Arias, Anna Epp, Xiaoxue Xu, and Catherine Choi. Thank you for the in-lab and out-of lab learning experiences and laughter that have been shared these past years. Your encouragement throughout my graduate experience has been whole-heartedly appreciated. Lastly, I would like to thank all other members of the lab that have supported me throughout the duration of my time including Naomi Fuglem and Adrianna Gunton, and Michelle Kim, for balancing the graduate-student pressures with your bright spirits. My daily determination reflected the motivational atmosphere facilitated by a positive team dynamic.

Thanks to Christine Fontaine, for co-founding the Neuroscience Graduate Student Association. You have fostered an environment of excellence and compassion amongst our fellow students. You have been not only a kind friend, but also a valued peer mentor.

A sincere thank you goes to my most dedicated friends during this time, Amanda McLaughlin, Patrick Reeson, Kara Ronellenfitch, Ben Murphy-Baum and Alex Hoggarth who have taught me strength and resilience. Thank you for all the hours spent climbing walls – literal rock walls, but also academic walls that have proved to be equally, if not

more, difficult to climb. Thanks to my family, for all the unconditional love and support you have given me in pursuit of my academic and research experiences.

1 Introduction

1.1 Thesis overview

Ankyrin-B (Ank-B) is a large 250 kDa cytosolic protein, known for its role as a scaffold for critical ion channels and transporters. Scaffolding proteins facilitate the organization and localization of proteins, ensuring the proper timing of signaling pathways (Chudasama, Marx, & Steinberg, 2008; Vondriska, Pass, & Ping, 2004). Although previous literature outlined the importance of Ank-B in the context of regulating the activity of binding partners (Mohler, Healy, et al., 2007; Mohler, Le Scouarnec, et al., 2007), the mechanism by which Ank-B itself is regulated, and how it contributes to specific cellular behaviours such as cell growth and differentiation are unknown.

My thesis explored a novel disease-causing mutation in the gene encoding for Ank-B resulting in expression of Ank-B p.S646F. The p.S646F mutation is a point mutation from a polar serine to a nonpolar phenylalanine residue. Amino acid 646 is located within Ank-B's Membrane Binding Domain (MBD), the region which acts as a binding site or scaffold for integral membrane proteins. Initial *in silico* analysis of the DNA sequence variant (*ANK2* c. 1937 C>T) predicted deleterious impact on the Ank-B protein. Due to the significant size and charge difference of the amino acid substitution, **I hypothesized that the p.S646F mutation in the MBD impacts on Ank-B proteostasis, which, in turn could result in abnormal cellular behavior(s)**. Protein homeostasis, or "proteostasis" is the concept that many biological pathways work in parallel and in

competition with each other to control the processes of biogenesis, folding, trafficking, and degradation of proteins in the cell. My thesis work uncovered key facets of the regulation, and dysregulation, of Ank-B proteostasis.

In Chapter 2, I outlined the *in vitro* techniques used to compare wildtype and mutant Ank-B. In Chapter 3, I described my findings on the characterization of Ank-B proteostasis as well as the impact of p.S646F on the regulation of Ank-B proteostasis, published in part in (Swayne et al., 2017). Based on the location and predicted negative effect of the mutation, I *hypothesized that p.S646F decreases levels of Ank-B*. I confirmed this hypothesis by performing transfections of a cardiomyoblast cell line with wildtype and p.S646F Ank2-GFP constructs and show that p.S646F reduced the amount of Ank-B in both cell types. I further *hypothesized that Ank-B degradation is regulated by the proteasome, and that the p.S646F mutation increases the degradation of Ank-B.* Despite some experimental caveats, my results suggested that rate of degradation of p.S646F was reduced compared to wildtype, and this degradation process was mediated by the proteasome. I also showed that the increased degradation of Ank-B associated with p.S646F was reduced by proteasomal inhibition. Overall, these results suggested that degradation of Ank-B by the proteasome was increased by the p.S646F mutation.

Because Ank-B has previously been linked to cardiomyocyte development, and patients harbouring the p.S646F mutation exhibit structural heart defects, in Chapter 4, I *hypothesized that the reduction of Ank-B by p.S646F alters cardiomyocyte growth and differentiation.* The effects of dysregulated Ank-B proteostasis were examined by characterization of cardiomyocyte cell proliferation rate, cell viability, and activation of differentiation pathways in cells with wildtype Ank-B overexpression, or with the

p.S646F mutant. Doubling time of wildtype and mutant Ank-B expressing cells were the same, but p.S646F mutation reduced overall cell counts over time. This decrease in cell count was attributed to an initial decrease in cell viability. Since the processes of cell viability and differentiation are closely related, I then compared expression of established differentiation markers. Expression of p.S646F Ank-B was shown to modulate the expression of differentiation markers compared to wildtype. Therefore, p.S646F mutation reduced cell viability and modulated expression of differentiation markers.

Lastly, in Chapter 5, I presented a general discussion of my results and the implications of my findings, focusing on how this work has expanded our understanding of Ank-B. I also proposed experiments and possible directions for future Ank-B research. Overall, this thesis provides new insight into how Ank-B protein levels are regulated, suggesting a new and critical role in cell differentiation. Specifically, the proteostasis and function of Ank-B is shown to be altered by a novel MBD mutation, and dysregulation of Ank-B leads to cellular changes that manifest into disease.

1.2 Proteostasis

Proteins are major cellular macromolecules responsible for establishing and modulating cell morphology, signal transduction, and overall cell function. The expression level of a protein in the cell at any given point in time is determined by the balance of transcription, translation, post-translational modifications, degradation. The net outcome of these simultaneously occurring processes underlies proteostasis – also known as *pro*tein homeo*stasis* (Figure 1.1). Proteostasis is essentially the life cycle of a protein, beginning with its generation to its eventual degradation. There are several recent comprehensive reviews of proteostasis (Alvarez-Castelao, Ruiz-Rivas, & Castaño, 2012;

Díaz-Villanueva, Díaz-Molina, & García-González, 2015). Gene transcription marks the start of a protein's life cycle. Next, after pre-mRNA processing, mature mRNA is transported to the cytoplasm. In the cytoplasm, ribosomes translate the mRNA into a nascent polypeptide. Primary, secondary, tertiary and quaternary structures of the protein are then developed by various post-translational modifications and protein-protein interactions. Importantly, aberrant conformations can occur due to standard overuse of proteins in the cell, but also due to genetic mutations. Protein misfolding associated with mutations or overuse can alter cellular proteostasis (Bianchini et al., 2014). Mutations causing conformational changes or alteration in protein-protein interactions can lead to aggregation, which via cellular chaperone systems targets them for degradation (M. Wang & Kaufman, 2016). The major degradation pathways are the Ubiquitin-Proteasome System (UPS) and the lysosomal pathway. Briefly the proteasome is a large multiprotein complex where cytosolic proteins are targeted via addition of poly-ubiquitin modifications. A complex system of proteins recognizes these modifications and shuttle such proteins to the proteasome for proteolytic degradation. The lysosome is where transmembrane proteins are degraded and it is an extension of the endocytosis system. Specific trafficking proteins will target protein cargo to the lysosome for degradation (Díaz-Villanueva et al., 2015). The cell responds to internal or external changes by modulating proteostasis of any given protein. In turn, the levels of a protein can activate signaling cascades to either maintain or amend the existing cell fate, and therefore, consideration of proteostasis is critical in understanding protein function in the cell.

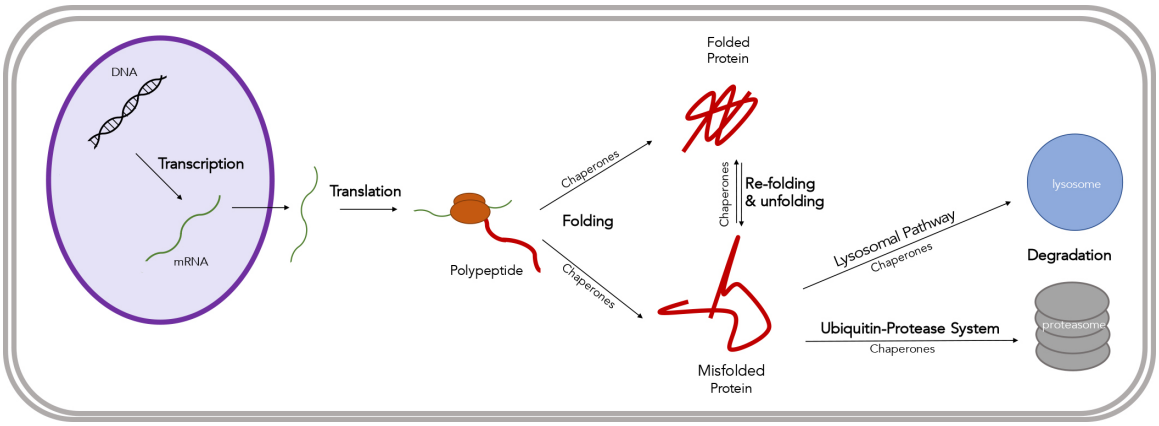

Figure 1.1 Processes underlying proteostasis and the unfolded protein response in the cell. Proteostasis begins with DNA transcription into mRNA. Mature mRNA is then transported to the cytoplasm where it is translated, forming the nascent polypeptide. The polypeptide is then subject to folding, via chaperone proteins, and develops its native 3-dimensional conformation. In the case of misfolded or unfolded proteins, the unfolded protein response is activated and recruits chaperone proteins that recognize and target proteins for re-folding and/or to the lysosome or proteasome for degradation.

1.2.1 Protein quality control and the unfolded protein response

How does the cell modulate and maintain proteins between the processes of synthesis and degradation? Protein Quality Control (PQC) is the process by which the cell responds rapidly to perturbations in the proteomic environment. This process monitors the quality, and quantity, of proteins throughout their lifespan (Buchberger, Bukau, & Sommer, 2010). The central players in the PQC are chaperone proteins, serving as mediators in multiple parts of the PQC. Chaperone protein function includes identifying misfolded or aggregated proteins and recruiting other chaperone proteins to target abnormal proteins for ubiquitination and degradation. Additionally, certain chaperones are involved in recycling, or refolding of abnormal proteins (Hetz, Martinon,

Rodriguez, & Glimcher, 2011; Oikawa, Kitamura, Kinjo, & Iwawaki, 2012; Schröder & Kaufman, 2005).

Perturbations in protein-folding homeostasis lead to the activation of the cell's Unfolded Protein Response (UPR), a part of the cell's PQC. The UPR is a collection of intracellular pathways that are recruited in response to the changes and requirements in protein-folding in the cell (Ron & Walter, 2007). Unfolded proteins trigger chaperone-protein mediated activation of 3 proximal detectors of the UPR: Protein kinase RNA-like ER kinase (PERK), Activating transcription factor 6 (ATF6), and Inositol-requiring protein 1a (IRE1) (Z. Wang & Hill, 2015). The activation of these receptors initiates multiple signal transduction pathways controlling downstream transcription factors and cell function (For full review, see Cornejo et al., 2013). Briefly, UPR receptors activation leads to reduction in global mRNA production to decrease ER stress associated with misfolded protein accumulation. UPR receptor activation also promotes the transcription of mRNA that increase the production of ER chaperones responsible for protein folding. Lastly, UPR activation can increase transcription of molecular chaperones involved in the ER-Associated Degradation (ERAD), to target misfolded proteins for degradation (Z. Wang & Hill, 2015).

ERAD is an adaptive pathway with specific chaperone proteins, known as E3 ubiquitin ligases, recruited in response to the presence of terminally misfolded proteins. These E3 ubiquitin ligases identify misfolded cytosolic proteins at specific sites of the cell, including organelles such as the ER (Buchberger et al., 2010). E3 proteins, or other chaperones systems such as HSP70 and 90, transport misfolded proteins to the cytosol to be ubiquitinated and degraded by the proteasome (Buchberger et al., 2010). Prolonged

activation of the UPR can lead to activation of apoptotic pathways, leading to cell death and chronic disease (Díaz-Villanueva et al., 2015; M. Wang & Kaufman, 2016).

In summary, the UPR is upregulated in response to misfolded protein accumulation. The UPR recruits chaperone molecules necessary for folding and re-folding of proteins, while also preventing the accumulation of misfolded protein aggregates by promoting their degradation. Therefore, depending on relative and concerted activation of each UPR pathway, the fate of the protein, and the fate of the cell, can be altered.

1.3 Cardiomyocyte development

Cardiomyocytes are muscle cells of the heart. The heart contains 4 compartments: right atrium, left atrium, right ventricle and left ventricle. These chambers compartmentalize oxygenated and de-oxygenated blood, pumping blood through the lungs to become oxygenated and then out to the body to provide oxygen to tissues. The heart is primarily composed of two types of cells: cardiomyocytes and cardiac pacemaker cells. Cardiac pacemaker cells are responsible for the generation of electrical impulses through the heart, ensuring rhythmic contraction of the left and right atrium followed by the left and right ventricles. Cardiac pacemakers are concentrated in the sinoatrial (SA) node) and spread through the ventricles via the electrical conduction system composed of the bundle of His and Purkinje fibers. The electrical impulses generated by the cardiac pacemaker cells initiate contraction of cardiac muscle, also known as cardiomyocytes. Cardiomyocytes are the critical cell type for the pumping action of the heart, and are the primary cell-type studied in this thesis.

During embryonic development, the heart generates cardiomyocytes by two processes: 1) differentiation of cardiac precursors (also known as cardiomyoblasts), and 2) division of existing mature cardiomyocytes (Foglia & Poss, 2016) (Figure 1.2). In the chick heart, cardiomyoblast differentiation forms a linear array along the cardiac tube prior to embryonic day 8.5 (E8.5), followed by rapid cell division producing clusters of early cardiomyocytes (Mikawa & Fischman, 1992). This transition between cardiomyoblast to early cardiomyocyte occurs a E10.5 – E14, corresponding to the formation of the mouse heart and rapid cardiomyocyte proliferation (Foglia & Poss, 2016). After birth, extensive early cardiomyocyte division occurs in postnatal mice from P0 – P7, allowing the heart to grow to adult size. During this time, the mammalian heart transitions from the immature proliferative state (early cardiomyocyte) to a mature hypertrophic state (late/mature cardiomyocyte) (Figure 1.2) (Dambrot, Passier, Atsma, & Mummery, 2011). When injuries are introduced between P0 – P7 substantial recovery is possible suggesting the proliferation state of the heart may also be compensatory and protective (Porrello et al., 2011).

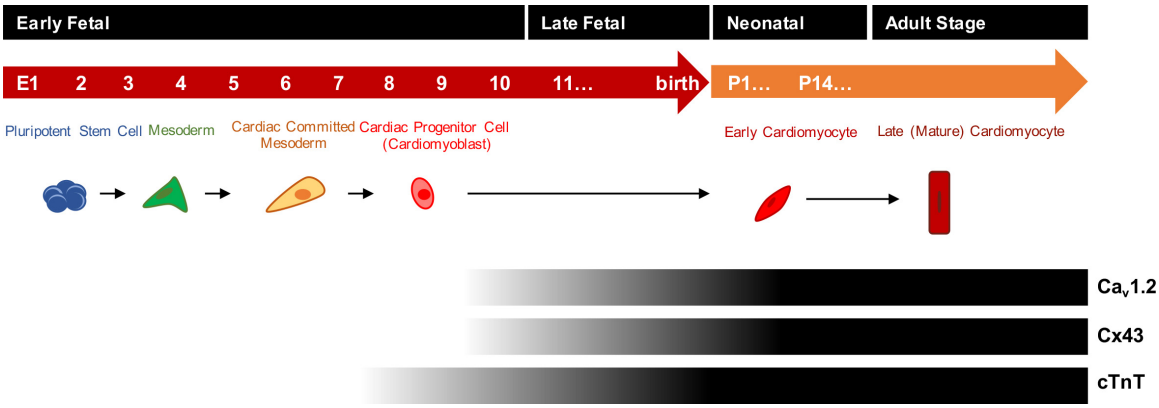

Figure 1.2 Differentiation of pluripotent stem cell into cardiomyocyte with reference to mouse embryonic and postnatal timeline. Pluripotent stem cells differentiate in mesodermal cells. Mesodermal cells become cardiac committed mesoderm cells which turn into cardiac progenitor cells, also known as cardiomyoblasts. Cardiomyoblasts become early cardiomyocytes which have increased expression of ion channels such as L-Type Ca^{2+} channel ($Ca_v1.2$), gap junction proteins such as connexin 43 (Cx43), and structural marker such as cardiac troponin T (cTnT). Early cardiomyocytes develop into late cardiomyocytes, which exhibit myofibril organization, sarcomeric striations, and mature electrophysiological machinery.

In contrast to development, in the adult mammalian heart, the population of cardiomyocytes with proliferative capacity dramatically decreases and is insufficient to completely repair damage (Bergmann et al., 2009; Kajstura et al., 2010; Porrello et al., 2011). Inability to repair the injury and increased cardiac load causes the heart to compensate by activating molecular pathways involved in hypertrophy (enlargement of cardiomyocytes). Cellular hypertrophy can lead to cardiomyopathy, thereby leaving the heart vulnerable to arrhythmia and cardiac failure (Foglia & Poss, 2016). The molecular mechanisms underlying the transition and confinement of the mature cardiomyocyte into a non-proliferative and hypertrophic state is poorly understood. Previous studies have

linked the transition from early to adult cardiomyocyte with the exit of the cell cycle, via inhibition of factors promoting cell division and upregulation of hypertrophic related pathways (Branco et al., 2015; Foglia & Poss, 2016; Watkins, Borthwick, & Arthur, 2011). Greater understanding of the molecular players involved in the transition from cardiomyoblast to early cardiomyocyte, and early cardiomyocyte to mature/late cardiomyocyte can help to unravel the etiology of developmental disease.

Inherited mutations that disrupt cardiomyoblast viability and/or the cardiomyoblast to cardiomyocyte transition could therefore impact on the development of mature heart structure, adaptive responses to stress, as well as repair capacity. These problems in turn could manifest in impaired structure and/or conduction/rhythm deficits. In this thesis, I explore the potential role of a mutant in a critical cardiac protein, associated with structural, conduction and rhythm deficits in humans, in the proliferation and development of cardiomyoblasts.

1.3.1 Cell culture models for cardiomyoblast development

The biological underpinnings of development of immature cardiomyoblasts into mature cardiomyocytes are poorly understood. Thus, cardiomyocyte development is often studied *in vitro* in simplified cell culture models to allow for observation of cellular behaviours, such as proliferation, differentiation and viability, across time. Two immortalized cell lines commonly used are: Hl-1 mouse atrial derived cells (Claycomb et al., 1998), and H9c2 rat embryonic ventricular derived cells (Kimes & Brandt, 1976). H9c2 cells are flat, large, and elliptically elongated (Kuznetsov, Javadov, Sickinger, Frotschnig, & Grimm, 2015). H9c2 cells proliferate, a characteristic of cardiomyoblasts; whereas mature primary cardiomyocytes are non-proliferative. To remain in a

proliferative state, however, H9c2 cells must not be allowed to reach 100% confluence or be over-passaged (Witek et al., 2016). Despite these challenges, H9c2 closely model primary neonatal cardiomyocytes in terms of membrane morphology, electrophysiological properties, and energy metabolism (Branco et al., 2015; Kuznetsov et al., 2015; Watkins et al., 2011), and can be fairly readily transfected, thus making them my cell model of choice. Furthermore, recent studies identified transcriptional changes in retinoic acid (RA)-induced differentiation of H9c2 reflect the hypertrophic state of the mature cardiomyocyte phenotype (Branco et al., 2015). Therefore, the differentiation of H9c2 cardiomyoblasts serve as an appropriate model to study ventricular cardiomyocyte development.

1.4 Ankyrin family of scaffold proteins

Ankyrins are a family of intracellular adaptor proteins that link integral proteins of the plasma membrane or endoplasmic reticulum to the spectrin-based cytoskeleton. In 1979, Vann Bennett & Stenbuck discovered the first ankyrin (ankyrin-R; Ank-R)(Vann Bennett & Stenbuck, 1979; V Bennett & Stenbuck, 1979). They ascribed it a primarily structural role due to its association with the erythrocyte cytoskeleton component, spectrin. Subsequent studies revealed other ankyrin types (Ank-B and -G) and multiple pathways in which ankyrins family proteins are required for both development of cell structure and localization of functionally related proteins (Vann Bennett & Healy, 2008, 2009). Further research has expanded our understanding of ankyrin proteins from exclusively structural or scaffolding proteins, to proteins that are ubiquitously expressed and crucial for the function of many cell types, particularly cardiomyocytes (Mohler, Gramolini, & Bennett, 2002).

There are 3 known ankyrin genes, *ANK1, ANK2,* and *ANK3,* which correspond to protein names Ank-R, -B, and -G, respectively. Ankyrins contain 3 functional domains (Figure 1.3): the membrane-binding domain (MBD), spectrin binding domain (SBD), and regulatory domain (RD) (Vann Bennett & Healy, 2008, 2009). The MBD consists of 24 ankyrin-motif repeats and, despite its name, does not directly bind the membrane but rather binds specific transmembrane proteins, anchoring them to the specific subcellular membranes such as the plasma membrane and sarcoplasmic reticulum (Vann Bennett & Healy, 2008, 2009). These specific loci are determined by the binding of the SBD to cytoskeletal structures, including various spectrin proteins. The RD consists of both a highly conserved death domain and a divergent C-terminal domain (Abdi, Mohler, Davis, & Bennett, 2006). Though the function of the C-terminal domain remains elusive, a study by Abdi and colleagues revealed that phosphorylation of this region modulates the strength of association between the MBD and ankyrin binding partners (Abdi et al., 2006).

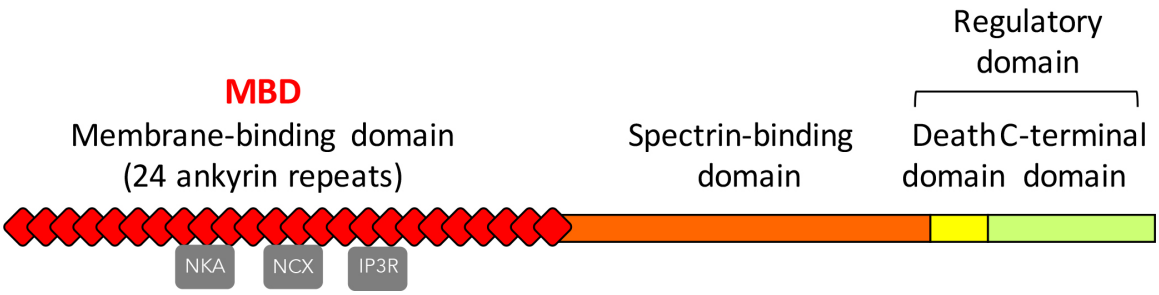

Figure 1.3 Ank-B structural domains. Ank-B is a large 250 kDa protein containing 3 structural domains: N-terminal or Membrane Binding Domain (MBD), Spectrin-Binding Domain (SBD), and Regulatory Domain (RD). The Regulatory Domain contains both the Death Domain (DD) and the C-terminal Domain (CTD).

Structural differences between ankyrin types contribute to their divergent functions. While structural similarities exist between ankyrin MBDs and SBDs, and all ankyrins function as protein-binders, ankyrins expressed in different tissues bind to different families of ion channels/transporters and cytoskeletal proteins (Abdi et al., 2006). The RD is the region that diverges most in sequence homology between types of ankyrins. Additionally, and perhaps not surprisingly, the RD plays a role in the modulation of MBD and SBD activity (Abdi et al., 2006; Vann Bennett & Healy, 2009). Indeed, the consistency in general function of each domain is fundamental for all ankyrins regardless of tissue, but sequence variation and differences in protein expression across cell types confers a diversity in the roles played by ankyrins.

1.4.1 Ankyrin function in the heart

The main function of cardiomyocytes is to contract to pump blood through the heart. Ank-B and Ank-G are highly expressed in cardiomyocytes (Uhlén et al., 2015), where they scaffold ion channels and transporters critical for the generation and propagation of action potentials (APs) that underlie contraction. Their MBD is responsible for the scaffolding role (Figure 1.4). Ank-B interacts with L-type channel ($Ca_v1.3$), Na^+K^+ATPase (NKA), inositol tri-phosphate receptor (IP3R), and Na^+Ca^{2+}Exchanger (NCX1). Ank-G expression is required for $Na_v1.5$ expression on the cardiomyocyte surface which mediates Na+ influx during the cardiac AP. Ank-G also interacts with critical proteins of the intercalated disc including plakophilin (PKP2), and connexin 43 (Cx43), (Mohler, Rivolta, et al., 2004). As Ank-B is the focus of my thesis work, the remainder of this section is focused on its role (Figure 1.4).

1.4.2 Ank-B regulates ion channel and transporter localization and intracellular Ca^{2+} homeostasis in the heart

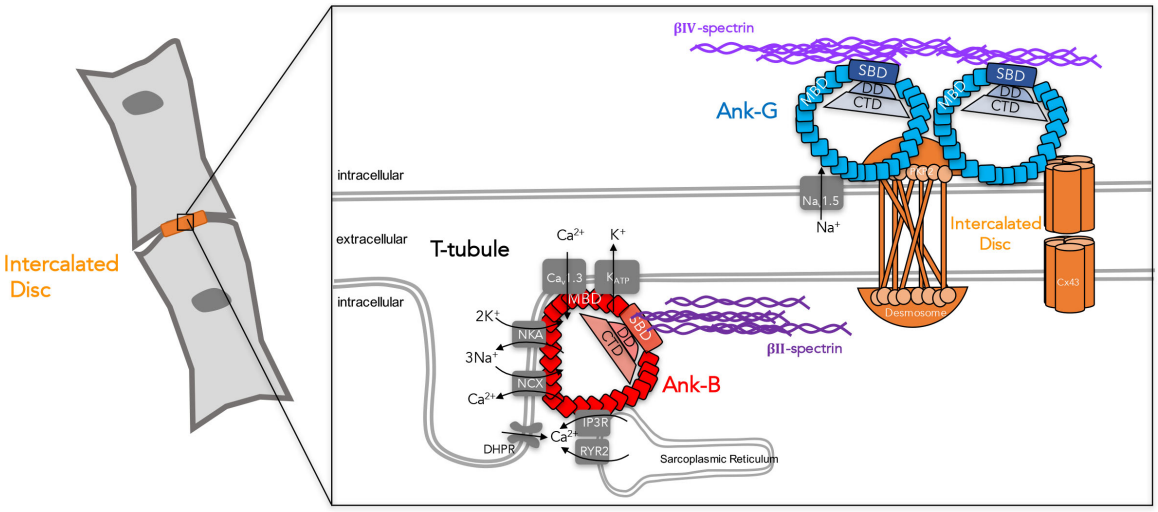

Figure 1.4 Ankyrins and key associated proteins in T-tubule and intercalated disc structure in cardiomyocytes. Ank-B controls the expression and localization of a tri-partite complex necessary for Ca^{2+} homeostasis and T-tubule formation: Na^+K^+ATPase (NKA), Na^+ Ca^{2+} Exchanger (NCX1), and Inositol 1,4,5-Triphosphate Receptor (IP3R). Ank-B also tethers ion channels $Ca_v1.3$ and K_{ATP} to the cardiomyocyte surface. Intercalated disc structure requires Ank-G mediated plakophilin-2 (PKP2) interactions and Connexin-43 (Cx43) gap junction stability.

Ionic homeostasis does not rely exclusively on ion channels and transporters of the plasma membrane; it is additionally maintained by a combination of mechanisms controlling intracellular Ca^{2+} levels. Ca^{2+} homeostasis establishes a defining feature of the cardiomyocyte action potential: its prolonged depolarization (approximately 200-400ms). This prolonged depolarization is mediated by influx of extracellular Ca^{2+} through voltage-gated L-Type Ca^{2+} channels (Figure 1.4). Ca^{2+} influx activates intracellular receptors,

IP3R and RyR, to release Ca^{2+} from intracellular sarcoplasmic reticular storage (Figure 1.4). This Ca^{2+} induced Ca^{2+} release underlies excitation-contraction, by which Ca^{2+} dependent proteins mediate actin and myosin interactions to shorten the sarcomere. Following excitation-contraction is repolarization-relaxation, mediated by the export and sequestering of Ca^{2+} into intracellular storage compartments (Brette & Orchard, 2003; Scriven, Dan, & Moore, 2000). Ank-B is the intermediary for controlling expression and localization of the so-called 'tripartite' complex of ion channels and transporters embedded in the cardiomyocyte plasma membrane and sarcoplasmic reticulum. This tripartite complex consists of the $Na^{+}K^{+}$ATPase (NKA), the inositol tri-phosphate receptor (IP3R), and the $Na^{+}Ca^{2+}$Exchanger (NCX1) (Cunha, Bhasin, & Mohler, 2007; Hashemi, Hund, & Mohler, 2009; Mohler et al., 2003; Mohler, Davis, & Bennett, 2005). Therefore, Ank-B-mediated tethering of proteins controls the Ca^{2+} homeostasis essential for the precise excitation-contraction coupling of cardiac cells. Ank-B $^{+/-}$ SA-node pacemaker cells have been shown to express decreased $Ca_v1.3$ protein levels (the pore-forming subunit of one of the subtypes of L-type Ca^{2+} channels in the heart), which are crucial for the prolongation of the cardiac action potential (Cunha et al., 2011). Furthermore, primary atrial cardiomyocytes displayed reduced L-type Ca^{2+} current, causing shorter action potentials (Cunha et al., 2011). Ank-B has also shown to be necessary for the repolarization phase of the cardiac AP as it is required for expression and function of the $K_{ir}6.2$ subunit of the K_{ATP} channel in primary myocytes (J. Li, Kline, Hund, Anderson, & Mohler, 2010) (Figure 1.4).

In summary, in the heart, Ank-B plays a critical role in the localization of integral membrane proteins at the cardiomyocyte T-tubule required for many cardiomyocyte

functions: prolongation and repolarization phases of the action potential, excitation-contraction coupling, and Ca^{2+} homeostasis.

1.5 Ank-B and cardiac disease

Ank-B mutations in the SBD and RD lead to a spectrum of phenotypes including sinus node dysfunction, atrial fibrillation, and Long QT Syndrome (Cunha et al., 2011; Robaei, Ford, & Ooi, 2015; Swayne et al., 2017; Wolf et al., 2013).

1.5.1 Long QT Syndrome (LQTS)

Long QT Syndrome (LQTS) is a category of cardiac arrhythmia characterized by a prolonged QT interval corrected for heart rate (QTc) measured by electrocardiogram (ECG). The QT interval is the period between the Q and T wave of the electrical cycle of the heart, representing the time between the start of ventricular excitation to the end of ventricular repolarization. Congenital LQTS is relatively rare as it impacts only 1 in 2000 people within the population world-wide (Schwartz et al., 2009). Diagnosis of LQTS requires an assessment of the QT interval, where a QTc greater than 450 ms for men or 460 ms for women indicates a prolonged QT interval (Schwartz et al., 2009); however, the QTc recorded by electrocardiogram (ECG) can be unreliable as it is variable within an individual, in addition to age and gender playing a role in altering QT interval. Furthermore, it is difficult to diagnosis as sudden cardiac death can be the first manifestation of LQTS caused by ventricular arrhythmia and syncope.

Long QT Syndrome (LQTS1-14) have been linked to specific genes coding mostly for ion channels (Schwartz et al., 2009). The most common genetic causes are genes that encode ion channels, such as K^+ channels (*KCNQ1* and *HERG*), and Na^+

channels (*SCN5A*). Most genetic testing screens for these common LQTS types. The clinical features of a prolonged QT interval have been clearly linked to both pharmaceutical influence on ion channels (acquired LQTS) and genetic ion channel variation, hence LQTS has been described as a channelopathy.

1.5.2 Long QT Type 4 (LQTS4) and Ank-B syndrome

Long QT Syndrome Type 4 (LQTS4) is the first genetically inherited LQTS associated non-ion channel gene mutations (Alders, Bikker, & Christiaans, 2018; Yong, Tian, & Wang, 2003). LQTS4 was originally mapped to the Ank-B gene (Schott et al., 1995). Mohler and colleagues subsequently identified the first loss of function mutation (2003). The genetic variants leading to LQTS4 occur in the spectrin-binding domain (SBD) and regulatory domain (RD), exhibiting varying degrees of loss-of-function (Figure 1.4; Mohler, Le Scouarnec, et al., 2007). The prevalence of LQTS4 is a rare cause of LQTS (less than 1% of cases) and is not always included in routine genetic screening for LQTS (Alders et al., 2018). LQTS4 is distinct from other LQTS types in that it coincides with a broad spectrum of other clinical features, collectively referred to as “Ank-B Syndrome”. Additional pathologies associated with the syndrome include sinus node dysfunction and atrial fibrillation (Cunha et al., 2011; Robaei et al., 2015; Swayne et al., 2017; Wolf et al., 2013). The disease characteristics range from asymptomatic to severe impacts on primary cardiomyocyte function, with phenotypes that do not necessarily overlap across variants (Figure 1.5).

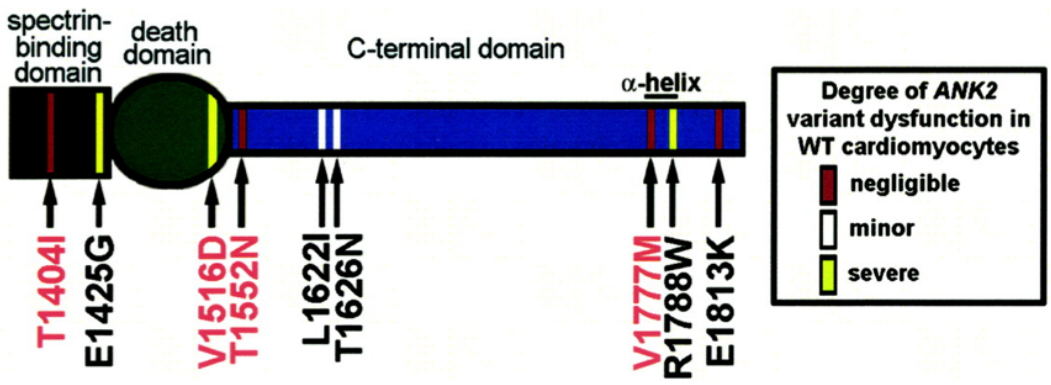

Figure 1.5 Human loss-of-function variants in Ank-B Spectrin Binding Domain (SBD), Death Domain (DD), and C-Terminal Domain (CTD) range in cardiomyocyte dysfunction severity. Nine human variants located in the SBD, and DD or CTD of the RD. Mutants were organized into 3 categories based on their effect on contraction rates and channel/transporter localization and/or expression in wildtype neonatal cardiomyocytes: 1) negligible (red box), indicates normal activity, 2) minor (white box), indicates loss-of activity, and 3) severe (yellow), indicating severe loss-of-function. Used with permission from (Mohler, Le Scouarnec, et al., 2007).

1.6 Identification of a novel LQTS variant in the Gitxsan First Nations of British Columbia

The Gitxsan, a First Nations Community in Northern British Columbia, exhibit a LQTS rate of 1:125 (Swayne et al., 2017) which is 15 times higher than the world-wide average (H. Jackson et al., 2011). Initial genetic screening identified a *KCNQ1* variant, p.V205M, linking many cases to LQTS1 (Arbour et al., 2008; H. A. Jackson et al., 2014). Further screening identified LQTS4 as an additional variant contributing to the high rate of LQTS in this population (Swayne et al., 2017). Specifically, this variant in the *ANK2* gene (*ANK2* c. 1937 C>T) results in a serine to phenylalanine substitution at

position 646 of the Ank-B protein (hereby referred to as the ‘p.S646F mutation’ or ‘p.S646F’).

The p.S646F mutation is the first known disease-causing variant located in the MBD of Ank-B (Figure 1.6). The position of this mutation in the MBD is likely important for Ank-B function as it is highly conserved across a range of invertebrate and vertebrate species (Swayne et al., 2017). The amino acid substitution of p.S646F results in a change from a polar to a non-polar residue which may have important functional consequences. Furthermore, *in silico* predictions with multiple platforms including MutationTaster, Polyphen, and PROVEAN foresee this variant as disease-causing/possibly damaging/deleterious (Swayne et al. 2017). It is reasonable to speculate that the rarity (Figure 1.7) and severity in physical presentation (Figure 1.8) of this novel variant could be attributed to the biologically significance of the MBD region.

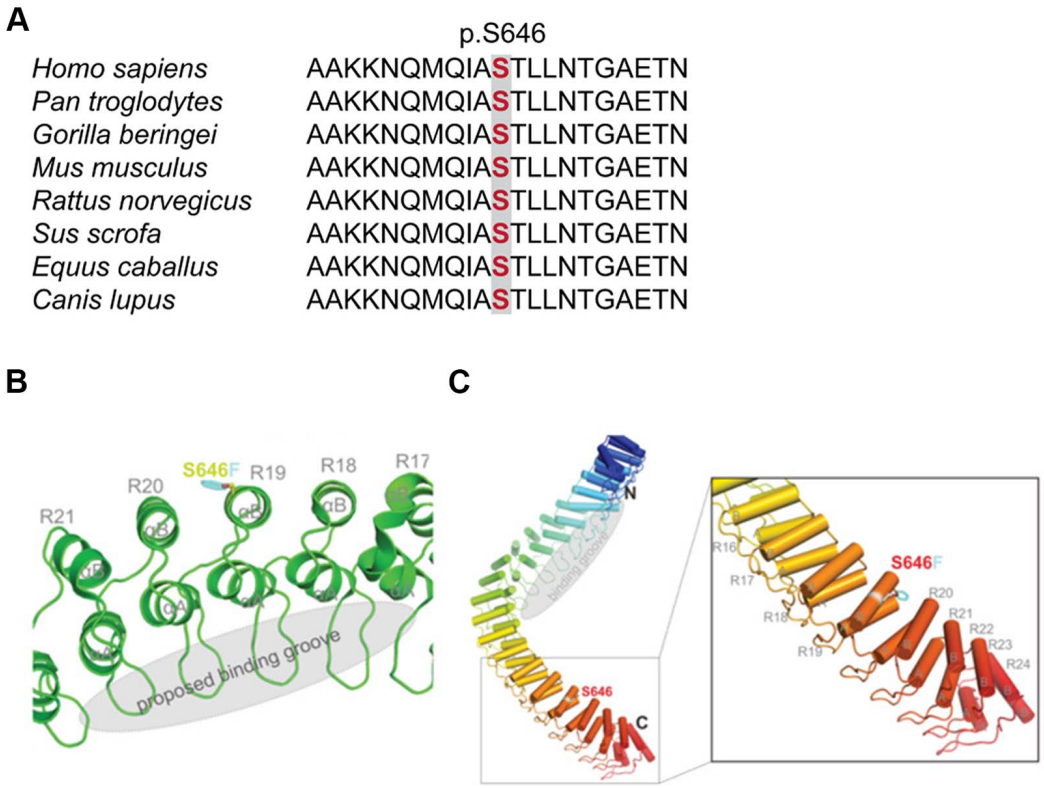

Figure 1.6 Ank-B p.S646F is in the membrane-binding domain and highly conserved across species. **A,** Ank-B conservation of S646 across vertebrate species. **B** and **C,** Location of p.S646F residue on the outer solenoid of the 19th ANK repeat of the MBD. Used with permission from (Swayne et al., 2017)

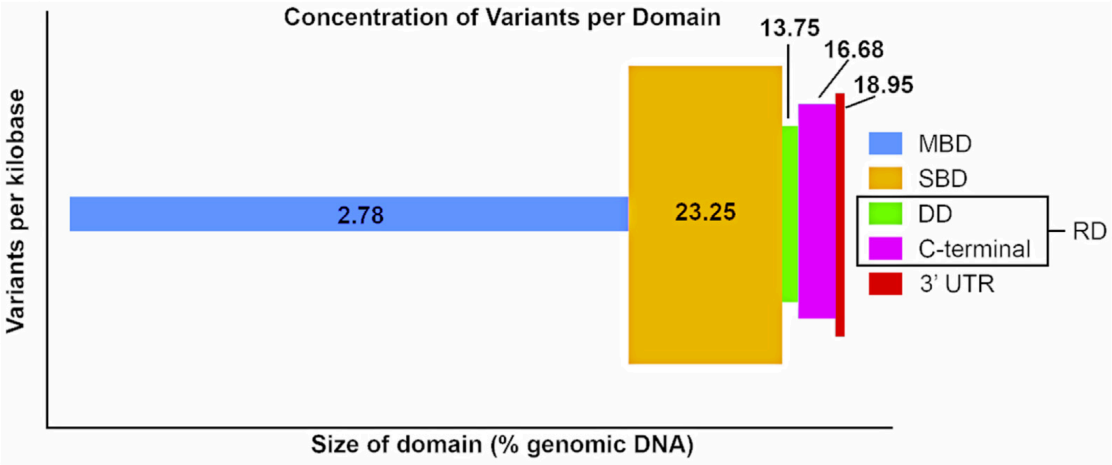

Figure 1.7 MBD contains the fewest variants in Ank-B. Over 2500 *ANK2* variants categorized by domain location. X- axis indicates the size of the domain represented as % genomic DNA. Y-axis displays average number of variants per kilobase per domain. MBD domain contains the lowest average number of variants per killobase of all domains. Used with permission from Koenig & Mohler, 2017.

Notably, the symptoms presented by this population differ from other loss-of-function Ank-B mutations, in that they range even broader than the typical Ank-B syndrome spectrum (Swayne et al., 2017). In addition to the classical presentation of a prolonged QT interval, syncope, and sudden cardiac death, the variant is associated with congenital cardiomyopathy, acquired dilated cardiomyopathy and additional conduction deficits (Wolff-Parkinson-White Syndrome; WPW), as well as seizures and cerebral aneurysms (Figure 1.8 and 1.9; Swayne et al., 2017). Therefore, compared to variants located in other domains of the Ank-B protein, the p.S646F variant of the MBD confers susceptibility to a more complex phenotype, that could involve cardiomyocyte, neuronal, and possibly, cardiovascular origins. The study of this mutation is important for understanding how changes in the MBD can lead to such varied presentations and

furthermore p.S646F serves as a key variant to study the importance of the MBD in Ank-B regulation and function at the cellular level.

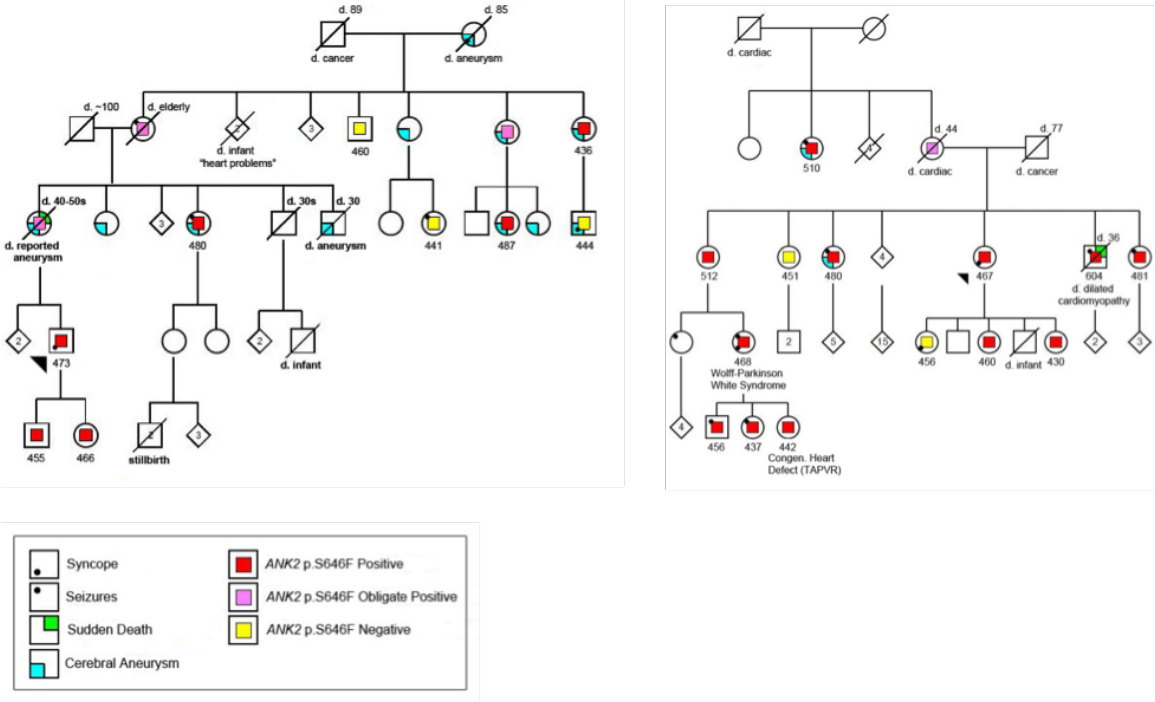

Figure 1.8 Pedigree of 2 multigenerational families with the *ANK2* p.S646F variant. The p.S646F variant is autosomal dominant in inheritance. The clinical features associated with the variant include syncope, seizures, sudden death, cerebral aneurysm, congenital cardiomyopathy (Total Anomalous Pulmonary Vein Return, TAPVR), adult onset cardiomyopathy (dilated cardiomyopathy), and accessory electrical systems (Wolff-Parkinson White Syndrome; WPW). Used with permission from Swayne et al. 2017.

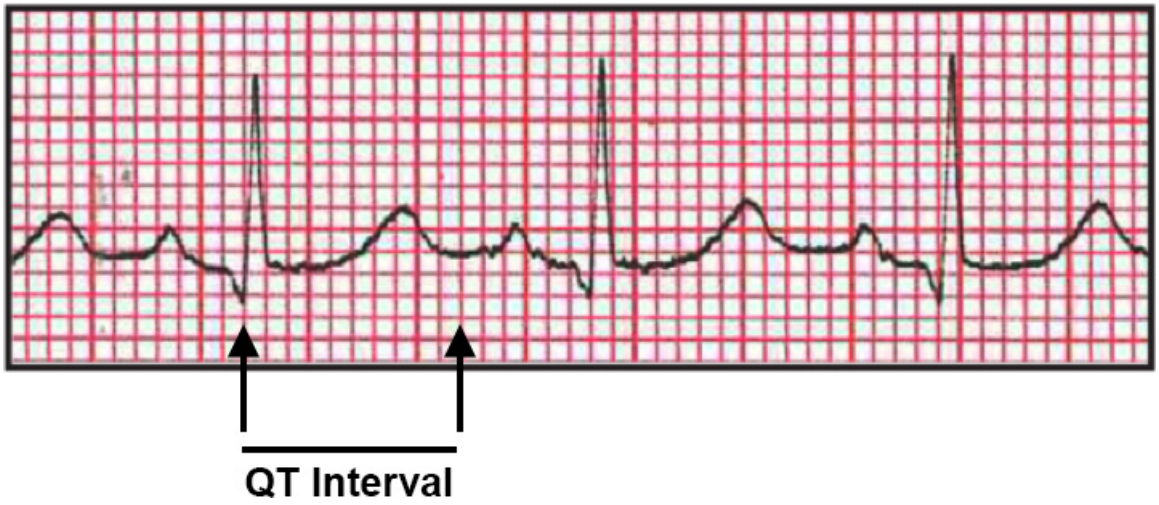

Figure 1.9 Electrocardiogram of LQTS phenotype of an individual positive for AnkB p.S646F. LongQT is a prolongation of QT interval, representing the duration of the depolarization to repolarization of ventricular caridomyocytes. QTc (QT interval corrected for heart rate) = 512 ms. Average QTc across individuals = 475 ms ± 40; range = 430-604 ms. Image used with permission from Swayne et al. 2017.

1.7 Summary of proposed cellular model: novel p.S646F MBD mutation dysregulates Ank-B leading to disease

Ank-B functions at the T-tubule regulating the conductive properties and synchronized contraction of cardiomyocytes by localizing key ion channels, receptors and transporters. Previous study of loss-of-function variants, revealed mislocalization of critical associated proteins results in irregular ion homeostasis such as decreased Ca^{2+} clearance, providing a model for p.S646F mediated prolonged QT interval. However, it is important to note that individuals harbouring the p.S646F variant exhibit a broader cardiac phenotype including cardiomyopathies and accessory electrical systems, suggesting p.S646F may play a role in development (Figure 1.8). Mouse cardiomyocytes

haploinsufficient for Ank-B exhibit abnormal properties, suggesting abnormal development (Mohler et al., 2003, 2005; Mohler, Splawski, et al., 2004). Furthermore, the serine residue at position 646 is highly conserved across species, with p.S646F being the first disease-causing variant in the MBD. Using various *in silico analyses*, p.S646F was predicted to be deleterious to the Ank-B protein. I therefore ***hypothesized that p.S646F affects Ank-B proteostasis impacting cellular function*** (Figure 1.10). My objectives were to 1) outline the mechanisms of Ank-B proteostasis, 2) elucidate cellular pathways that are interrupted by MBD loss-of-function variant p.S646F, and 3) determine how disruption of these pathways results could lead to changes in cellular function. This thesis spans these objectives in Chapter 3 and Chapter 4, confirming the prediction that p.S646F impacts Ank-B levels by interfering with its proteostasis, resulting in deleterious changes to cell growth and survival (Figure 1.10).

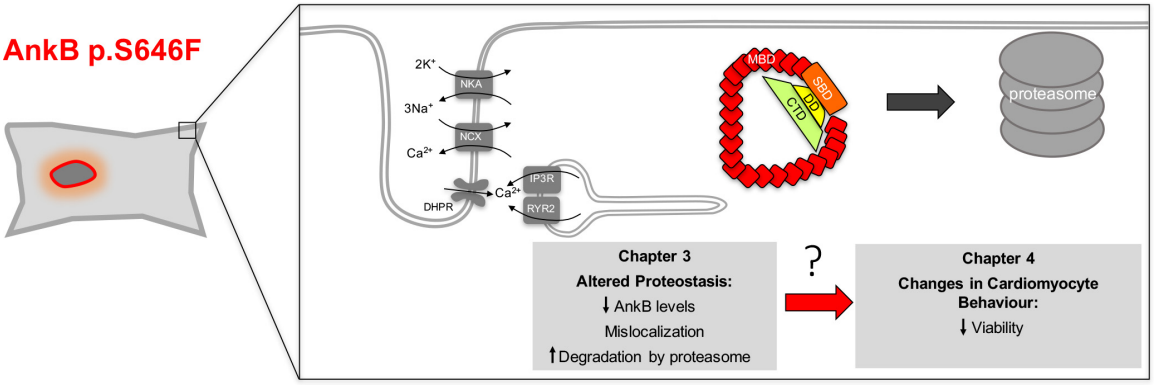

Figure 1.10 Summary of findings and working model of p.S646F effects on Ank-B proteostasis and cell function. In Chapter 3, I determined the proteasome is the primary pathway regulating Ank-B degradation. I also discovered S646F decreases Ank-B protein levels in cardiomyocytes by accelerating its rate of degradation by the proteasome. In Chapter 4, I uncovered the cellular behaviours Ank-B proteostasis underlies, viability, and differentiation. I then revealed p.S646F dysregulates Ank-B proteostasis, thereby disrupting these cellular behaviours and revealing the cellular and molecular mechanisms underlying Ank-B related disease.

2 Methods

2.1 Plasmids

The cDNA encoding the 220 kDa Ank-B isoform (*ANK2* isoform 2 [*Homo sapiens]*) was commercially synthesized and subcloned into pAcGFP-n1 (Bio Basic Inc. accession number NM_020977.3). The Ank-B p.S646F-GFP-encoding plasmid was created by site-directed mutagenesis of wildtype Ank-B-GFP constructs using a QuickChange II XL Site-Directed Mutagenesis Kit (Agilent Technologies) according to the manufacturer's protocol with the following primers (Integrated DNA Technologies): (Forward: 5'GAATCAATGCAGATAGCTTTCACACTCCTGAACTATGG-3'; reverse: 5' CCATAGTTCAGGAGTGTGAAAGCTATCTGCATTTGATTC-3'). Constructs were confirmed with sequencing (Eurofin Operon). All plasmids were confirmed by DNA sequencing (Eurofin Operon). Plasmid transformation was conducted in DH5α cells (Invitrogen) and plasmid preparation were prepared with CompactPrep Plasmid Midi Kit (Qiagen) according to the manufacturer's protocol.

2.2 Cell culture

2.2.1 Passaging

H9c2 *Ratticus norvegicus* ventricular derived myoblast and HEK293T *Homo sapiens* embryonic kidney cell lines were procured from the ATCC®. Cells were cultured in Dulbecco's modified Eagle's medium (DMEM), 10% fetal bovine serum (FBS), 100 U/mL penicillin, 100 µg/mL streptomycin (all from Gibco^{TM}/ Life Technologies) . H9c2 cells were plated at 500,000 cells per 15 cm plate and allowed to reach a maximum of

70% confluence before passaging every 3-4 days. HEK293T cells were seeded at $3.4x10^6$ cells per 10 cm plate and allowed to reach 80% confluence before passaging every 2-3 days.

2.2.2 Transfections

Cells were transfected with the wildtype Ank-B or p.S646F encoding plasmid plasmid as per jetPEI manufacturer's protocol (Polyplus-transfection® SA/VWR) 24 hours post-seeding unless otherwise indicated.

2.3 Cycloheximide Experiments

In Chapter 3, 24 h post-transfection, H9c2 cells were treated with 30 μg/mL cycloheximide (CHX; Sigma) to inhibit protein translation. Cells were collected at 0 hours and every 6 hours for 36 hours total.

2.4 Confocal Fluorescence Microscopy

HEK293T cells were plated on Poly-D-Lysine (PDL;Sigma)-coated glass coverslips. 24 hours after seeding, cells were transfected with the wildtype or mutant plasmids. Media was removed and coverslips were washed in Phosphate Buffered Saline (PBS; 77 mM Na_2HPO_4, 23mM NaH_2PO_4, and 1.5M NaCl). Cells were subsequently fixed in 4% paraformaldehyde (PFA) in PBS. Following fixation, coverslips were washed 3 times with PBS and incubated with the nuclear marker Hoechst 33342 (1:300; ThermoFisher Scientific), diluted in antibody buffer (3% w/v bovine serum albumin (BSA), 0.3% v/v Triton X-100 in PBS). Coverslips onto glass slides using Vectashield (Vector Laboratories). Images were taken at 20X (0.7 aperture; 512 X 512 logical size; 1.127 μm pixel size).

H9c2 seeding, transfection, treatment and time collection are according to the H9c2 differentiation marker protocol above, except performed on PDL-laminin coated glass coverslips (NeuroVitro). Cells were fixed with 4% PFA in PBS for 10 minutes at room temperature, and permeabilized with 0.1% Triton X-100 in PBS for 4 minutes. Slips were incubated in 5% BSA for 10 minutes. F-actin and nuclei were stained with Phalloidin Alexa Fluor 555 (1:40; Invitrogen) and Hoechst 3342 (1:100; Invitrogen). Stains were diluted in 1% BSA antibody buffer in PBS and slides were incubated for 40 minutes at room temperatures, rinsed with PBS, and mounted in VectaShield (Vector Labs). Images were taken at 20X (0.7 aperture; 1024 X 1024 logical size; 0.568 μm pixel size).

All microscopy was conducted using a Leica TCS SP8 confocal laser-scanning microscope. Images were taken in the confocal plane displaying the largest plane of the nucleus. Images were adjusted for contrast uniformly by Adobe Photoshop CS5 Extended software (CC 2015.12) for representative images only. No contrast adjustments were made prior to analysis and comparison were made between images acquired under identical conditions.

2.5 Degradation Pathway Experiments

In Chapter 3, Ank-B degradation pathway was determined by treating H9c2 cells with 0nM, 25nM or 50nM PS-341 (ThermoFisher Scientific) or 0 nM,10 nM or 25 nM Bafilomycin A (BafA; Sigma) 6 hours post-transfection with wildtype Ank-B-GFP, and collected 12 hours after inhibitor treatment. To test if Ank-B levels could be rescued by proteasomal inhibition, H9c2 cells were treated with 0 nM or 10 nM 6 hours post-

transfection with wildtype or Ank-B p.S646F-GFP, and collected 12 hours after PS-341 treatment.

2.6 Western blotting

Cells were homogenized with PBS-RIPA buffer (Phosphate buffered saline-Radioimmunoprecipitation assay (PBS-RIPA) buffer; 10 mM PBS [150 mM NaCl, 9.1 mM Na_2HPO_4, 1.7 mM NaH_2PO_4] 1.0% IGEPAL CA-630, 0.5% sodium deoxycholate, 0.1% sodium dodecyl sulfate (SDS)) or Tris-based RIPA buffer (150mM NaCl, 1.0% IGEPAL CA-360, 0.5% sodium deoxycholate, 0.1% SDS, 50 mM Tris, pH 8.0) supplemented with protease inhibitor cocktail (1 μL/1 mL RIPA (stock: 0.104 mM 4-(2 aminoethyl) benzenesulfoyl fluoride hydrochloride, 0.08 mM aprotinin, 4 mM bestatin hydrochloride, 1.4 mM n-(trans-epoxysuccinyl)-L-leucine-4-guanidinobutylamide, 2 mM leupeptin hemisulfate salt, 1.5 mM pepstatin A; Sigma Aldrich)), phenylmethylsulfonyl fluoride (PMSF) at 10 μL/1 mL RIPA, and 1 mM ethylenediaminetetraacetic acid (EDTA), passed through a 27-gauge needle twice and incubated for 30 minutes on ice to lyse and extract protein from cultured cells. To remove debris, cell lysates were centrifuged at 4°C for 20 minutes at 12,000 rpm and supernatant was collected. Samples were prepared with SDS-PAGE loading dye under reducing conditions (β-mercaptoethanol) and heated at (95°C) for 5 minutes prior to SDS-PAGE. Gels were transferred to a 0.3 μm pore-size polyvinyldene fluoride (PVDF) membrane for 2.5 hours at 0.2 A. Successful transfer of protein onto PVDF membrane was confirmed by Ponceau S total protein staining (%). Blocking incubations took place in 5% blocking buffer (5% skim milk in Phosphate Buffered Saline-Tween (PBS-T); 10mM Na_2HPO_4, 1.25 mM NaH_2PO_4, 2.7 mM KCl, 137 mM NaCl, 0.1% Tween 20) or Tris-based Buffered Saline-

Tween (TBST) 20 mM Tris, 150 mM NaCl, 0.1% Tween 20. Primary antibodies were prepared in 1% blocking buffer (1% skim milk powder in PBST or TBST) and secondary antibodies took place in PBST or TBST. Bands were visualized with Enhanced Chemilunescence (ECL; BioRad Laboratories, Inc.) or WestFemto (ThermoFisher Scientific). Relative chemiluminescence was quantified by densitometry measurements using ImageJ 1.45 software (http://imagej.nih.gov/ij/). All values were normalized to β-actin signal. Primary antibodies used included anti-β-Actin (1:4,000 – 1:16,000; Sigma), anti-$Ca_v1.2$ (1:500; Millipore), anti-Cx43 (1:1000; Cell Signalling Technology), anti-cTnT (1:500; Abcam); anti-GFP polyclonal (1:8,000 – 1:128,000; Life Technologies). Secondary antibodies were horseradish peroxidase (HRP)- conjugated AffiniPure donkey anti-rabbit IgG (1:2,000-1:4,000), HRP- conjugated AffiniPure donkey anti-mouse IgG (1:2,000-1:4,000; both from Jackson ImmunoResearch).

2.7 Proliferation assay

A preliminary study was performed to understand the typical growth curve of untransfected H9c2 cell line. H9c2 cells were plated at a density of 355 cells/cm^2. Trypan Blue (0.4% Trypan Blue in PBS; Stem Cell Technologies) was used in a 1:1 ratio of cell suspension to detect dead cells. Total cell, dead cell, and live cell counts (based on exclusion of trypan blue) were performed 6 hours after plating and every 24 hours for 96 hours using a hemocytometer. H9c2 untransfected cells exhibit a typical growth curve, with a doubling time of 30.43 h, reaching 1.3 x 10^5 cells in 96 h (Figure 2.1).

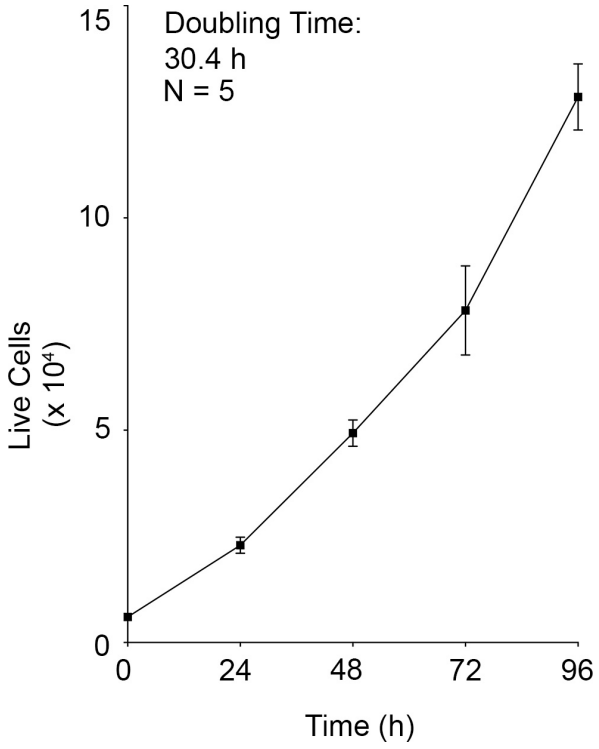

Figure 2.1 Untransfected H9c2 exhibit typical growth curve. Cells were re-plated 24 h post-transfection and live cells were counted with Trypan Blue Exclusion Dye 6 h after replating ("0h"), and every 24 h for 96 hours. Mean live cell numbers (x 10^4) are plotted. Log live cell numbers were used to determine the lag phase, 0 h –24 h, and exponential growth phase, 48 h – 96 h. Using the exponential growth phase (48 h – 96 h), a doubling time of 30.4 h was calculating, with cells reaching 1.3 x 10^5 cells in 96 h.

For wildtype and p.S646F comparison of proliferation rates in Chapter 4, H9c2 cells were re-plated 24 hours transfection at a density of 355 cells/cm^2. Live and dead cells counts took place 6 hours after re-plating and every 24 h after the initial counting, for 96 hours total.

2.8 MTT cell viability assay

In Chapter 4, to determine H9c2 cell viability, MTT Assay (3-(4,5-Dimethylthiazol-2-yl)-2,5-diphenyltetrazolium bromide (MTT) Assay; Vybrant® MTT Cell Proliferation Assay Kit; ThermoFisher Scientific) was used according to the manufacturer's quick protocol option. Briefly, cells were seeded in a 96-well plate at a density of 5.1×10^3 cells per well in regular maintenance medium and transfected 24 hours after seeding. At 48 hours post-transfection, cells were incubated in fresh maintenance medium supplemented with 10 μL of MTT solution (12 mM in PBS). A negative control contained 10 μL of MTT stock solution in 100 μL medium with no cells. The plate was incubated at 37 ℃ for 4 hours. After labelling, 25 μL of medium was removed from wells and 50 μL DMSO (dimethyl sulfoxide) was added to each well, thoroughly mixed, and incubated at 37°C for 10 minutes. After mixing each sample again, absorbance was read at 540 nm (Infinite®200 PRO microplate reader; Tecan Life Sciences).

A blank control (no cells) was subtracted from all absorption values. Two positive controls for cell viability were included: no transfection, and mock transfection in which the transfection protocol was carried out in the absence of DNA. A negative control for cell viability was also included in which cell viability was reduced by treatment with high dose of cycloheximide (300 μg/mL CHX; Sigma).

2.9 Differentiation marker expression

In Chapter 4, markers for cell death and differentiation were quantified in wildtype or p.S646F Ank-B-GFP transfected H9c2 cells using Western blotting. Positive

control for differentiation was H9c2 cells cultured in low-serum (1% FBS) medium supplemented with 10 nM all-*trans* retinoic acid (ATRA). Cells were seeded at 3,889 cells/cm^2 in full-media prior to incubation for 24 h prior to incubation with differentiation media For Ank-B expressing cultures, H9c2 cells were seeded at 8,333 cells/cm^2 and transfected with either wildtype or p.S646F Ank2-GFP plasmid 24 hours post-seeding. The culture medium was changed every 48 hours post-transfection with respective full or differentiation media. Plates, or slides, were collected 24 hours, 72 hours, and 120 hours after transfection/treatment for immunostaining or lysates for Western blot analysis.

2.10 Statistical Analysis

Statistical analyses were performed using Prism for Mac OS X (Version 7.0a, GraphPad software, Inc.). All values are reported as means, and all variances are reported as standard error of the mean. Significance is denoted as $P < 0.05$ (*), $P < 0.01$ (**), $P < 0.001$ (***), $P < 0.0001$ (****). Statistical tests and P values are reported in each figure legend.

3 Ank-B is degraded by the proteasome

The data in this Chapter has been published in part in Swayne LA, Murphy P, Asuri S, Chen L, Xu X, McIntosh S, Wang C, Lancione PJ, Roberts JD, Kerr C, Sanatai S, Sherwin E, Klin CF, Zhang M, Mohler P, Arbour LT. Novel variant in the *ANK2* membrane-binding domain is associated with Ankyrin-B Syndrome and structural heart disease in a First Nations population with a high rate of LongQT Syndrome. *Circulation: Cardiovascular Genetics.*10(1) doi:10.1161/CIRCGENETICS.116.001537.

3.1 Overview

Ank-B is a scaffolding protein necessary for the development of cardiomyocytes and their excitable nature (ability to fire action potentials). Consistently, p.S646F was associated with deficits in cardiovascular conduction in the patient population (Swayne et al., 2017). These effects encompassed cardiac LQTS-related atrial fibrillation, tachycardia and bradycardia, in addition to congenital accessory electrical pathways of the heart and cardiomyopathy (Swayne et al., 2017). The cellular mechanism(s) underlying abnormal cardiovascular phenotypes associated with AnkB p.S646F was an important knowledge gap when I began my thesis work.

Proteostasis is a cellular process encompassing all biochemical pathways occurring both sequentially and in tandem to regulate proteins levels in the cell (Buchberger et al., 2010; Díaz-Villanueva et al., 2015). This includes synthesis, folding, and degradation of proteins. Dysregulation during any part of proteostasis can lead to changes in protein levels, and function. Interestingly, the p.S646F mutation is a point mutation resulting in an amino acid substitution from a polar residue (S, serine) to a nonpolar residue (F, phenylalanine; Swayne et al., 2017). The abnormal exposure of hydrophobic residues can be targeted by systems of degradation in the cell (Cornejo et al., 2013; Hetz, Chevet, & Oakes, 2015), which can lead to changes in the homeostasis of the protein. *In silico* analyses outlined in Swayne et al. (2017) predicted p.S646F to be

deleterious to the Ank-B protein. *I therefore hypothesized that p.S646F Ank-B-GFP alters Ank-B stability in cells resulting in reduced expression levels.*

To test this hypothesis, I transfected cell lines with plasmids containing the genes encoding for wildtype or mutant (p.S646F) Ank-B and used Western Blotting to quantify Ank-B protein expression levels using an anti-GFP antibody. When expressed in the H9c2 rat ventricular cardiomyoblast cell line, mutant Ank-B levels were significantly lower than wildtype levels 48 hours post transfection. Notably, using HEK293T cells, I demonstrated that wildypte and mutant Ank-B were expressed at similar levels in this non-cardiomyoblast cell line. Next, I used a protein synthesis inhibitor to determine a time course of wildtype and mutant (p.S646F) Ank-B expression in the H9c2 cardiomyoblast cell line. I further investigated the mechanism in which Ank-B is degraded (proteasome vs lysosome), and determined whether blocking this mechanism could rescue mutant Ank-B protein levels.

3.2 Results

To begin to investigate the cellular mechanisms underlying cardiac dysfunction associated with Ank-B p.S646F, I first investigated the expression levels of wildtype and mutant Ank-B in the H9c2 cardiomyoblast cell line by Western blotting 48 hours post-transfection (Figure 3.1). I observed a significant decrease in the expression of mutant Ank-B relative to wildtype. These results suggested that p.S646F Ank-B protein levels were reduced in comparison to wildtype, when expressed in cardiomyoblasts *in vitro*. These findings were published in Swayne et al. 2017.

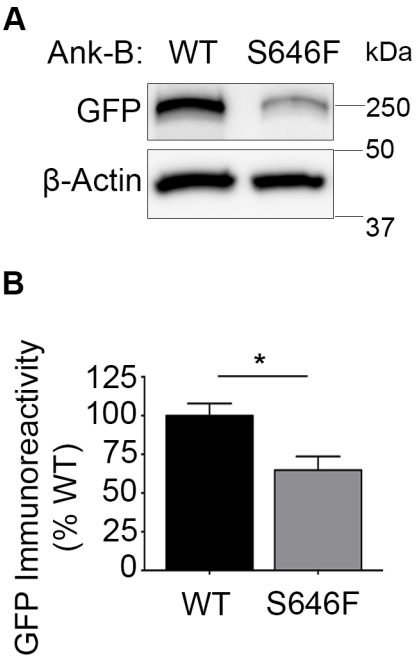

Figure 3.1 Ank-B p.S646F exhibits decreased levels of expression in the H9c2 rat ventricular cardiomyoblast cell line. A, Immunoblot of H9c2 lysates collected 48 h after transfection with either wildtype or p.S646F Ank-B-GFP plasmid. **B,** Quantification of Ank-B-GFP immunoreactivity normalized to β-actin, represented as % wildtype control levels ((*) $P = 0.0408$ by t-test; N = 3). These results are published in Swayne et al. 2017.

To next determine whether wildtype Ank-B and Ank-B p.S646F could be expressed in equivalent amounts in a non-cardiomyoblast cell line, I used HEK293T cells. HEK293T cells contain relatively low levels of endogenous Ank-B levels (Thul et al., 2017; Uhlén et al., 2015), and RNA expression according to the Cell Atlas of the Human Protein Atlas Collection (https://www.proteinatlas.org/ENSG00000145362-ANK2/cell) and Expression Atlas (https://www.ebi.ac.uk/gxa/home/). Like most mammalian cell lines, HEK293T are compatible with CMV-promoter induced expression from plasmids (Jaganjac et al., 2010; Qin et al., 2010). Immunofluorescence imaging

indicated that transfection efficiency wildtype were similar for wildtype Ank-B and Ank-B p.S646F in HEK293T cell line (wildtype: 100.0% ± 19.0, p.S646F: 132.4% ± 27.8; P = 0.3897 by t-test; Figure 3.2 A and B). Consistent with imaging results, Western Blot analysis (Figure 3.1 B and C) indicated similar expression levels between wildtype and p.S646F Ank-B (wildtype: 100% ± 11.4, p.S646F:114.8% ± 12.7; P = 0.4201 by t-test; Figure 3.2 C and D).

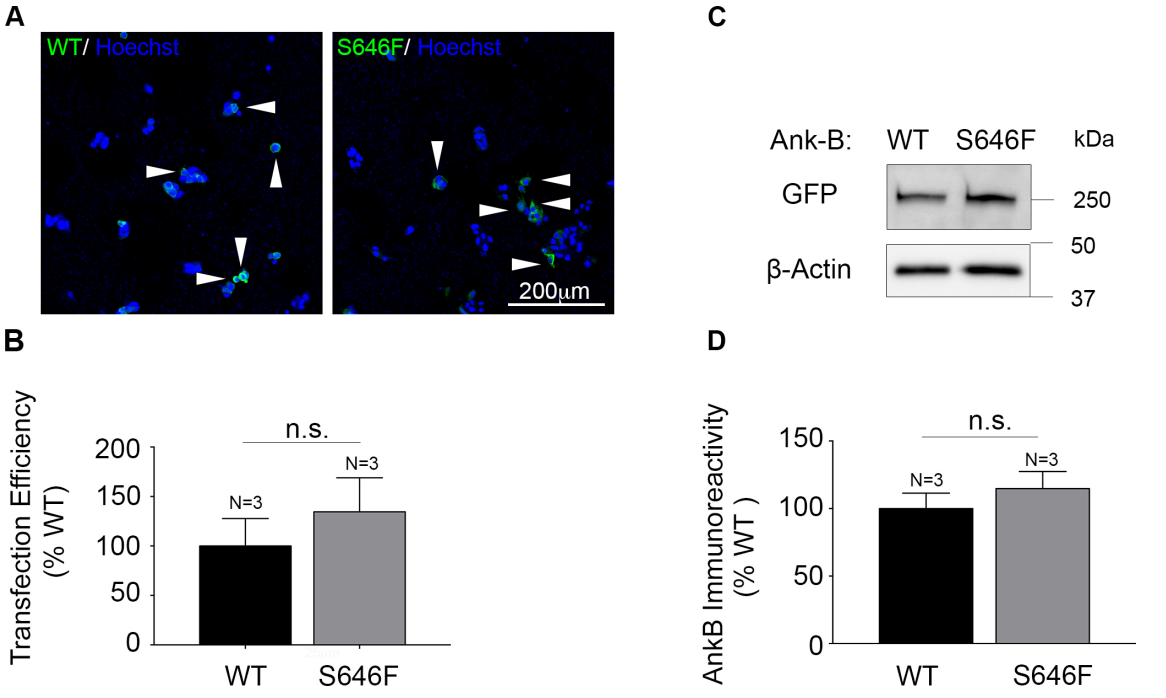

Figure 3.2 Wildtype and p.S646F plasmids exhibit similar transfection efficiencies and expression levels in HEK293T cells. A, HEK293T cells 48 hours after transfection with wildtype or p.S646F-GFP plasmid. Scale bar = 200 um. **B**, Quantification of transfection efficiency represented as % wildtype control, with no significant difference between wildtype and p.S646F-GFP transfected cultures (P = 0.3897 by t-test; N = 3). C**,** Immunoblot of HEK293T lysates expressing either wildtype or p.S646F-GFP collected 48 hours after transfection. **D**, Quantification of immunoblot GFP expression normalize to β-actin immunoreactivity, represented as % wildtype control levels. (P = 0.4201 by *t*-test, N = 4).

To gain more insight into the relative turnover rates of wildtype and mutant Ank-B in cardiomyoblasts, H9c2 cells were treated with protein translation inhibitor, cycloheximide (CHX) 24 hours after transfection (Figure 3.3). CHX binds to the large ribosome stopping *de novo* synthesis of Ank-B, thereby restricting our focus to the mature Ank-B protein, and its degradation over time. Wildtype and mutant Ank-B levels were determined by Western blotting of lysates collected every 6 hours (starting 24 hours post-transfection; 'time 0') for 36 hours. Note that at time 0 (before CHX) and 6 hours after CHX treatment, wildtype and mutant Ank-B levels were almost identical. A slight (albeit insignificant) increase in Ank-B levels for both wildtype (until 18 hours) and mutant (until 6 hours), suggested that the CHX did not initially fully halt all gene expression resulting from the transfected plasmid. This observation will be revisited in the Discussion for this chapter. Levels of mutant Ank-B-GFP levels were consistently lower than wildtype from the 12 hour time point onwards, however this difference was very small and although significantly different by two-way ANOVA for time and genotype, Bonferroni *post hoc* analysis showed no mean differences at any time point (Figure 3.3). Note that cells treated with CHX for longer than 36 hours were unviable and no samples could be reliably obtained. Therefore the 36 hour time point, where there is still substantial Ank-B expression (for both wildtype and mutant) was the latest possible analysis time point. This precluded accurate determination of the Ank-B half-life and suggest that it is longer than 36 hours. Overall, the inability to determine the accurate Ank-B half-life due to the deleterious effects of CHX on H9c2 cells, rendered this degradation analysis inconclusive. Furthermore, investigation of the literature on this type

of analysis revealed numerous possible confounding factors (Alvarez-Castelao et al., 2012) that will be discussed in depth in the Discussion section of this Chapter.

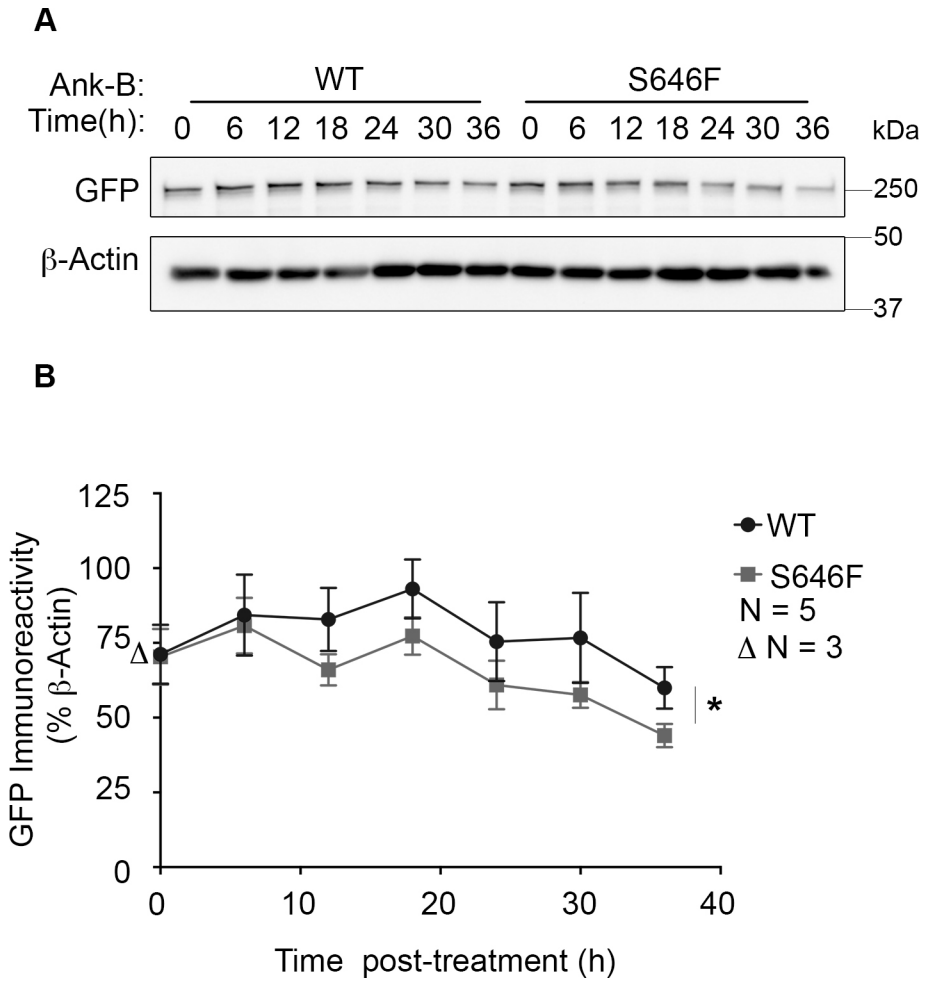

Figure 3.3 Time course of Ank-B expression with CHX treatment. A, Immunoblot of GFP-tagged wildtype and p.S646F Ank-B levels of H9c2 cells treated with CHX 24 h post-transfection and collected every 6 h post-CHX (CHX, 30 μg/mL) for 36 h. **B,** Quantification of GFP immunoreactivity expressed as a percentage of the corresponding β-actin signal. (Genotype: $F(1,48) = 6.686$, $P = 0.0128$; Time: $F(6,48) = 3.191$, $P = 0.0144$; Interaction: $F(6,48) = 0.9742$, $P = 0.165$ by two-way ANOVA of wildtype and p.S646F expression between from 6 h to 36 h; Bonferroni's multiple comparison indicate $P > 0.05$ for all time points).

I next focused on the mechanism of Ank-B protein degradation. Because Ank-B is a cytoplasmic protein, *I hypothesized that it undergoes proteasomal degradation*. To investigate this hypothesis, I first treated H9c2 cells expressing wildtype Ank-B with proteasomal and lysosomal inhibitors (Figure 3.4). H9c2 cells expressing wildtype Ank-B-GFP were treated with increasing concentrations of either the proteasome inhibitor PS-341 or lysosomal inhibitor Bafilomycin A (BafA) (Figure 3.4 A and B). PS-341 (also known as Bortezomib) binds to the catalytic site of the 26S proteasome to inhibit its action, while BafA binds to the vacuolar proton pump preventing fusion of autophagasomes and lysosomes, interfering with the lysosomal pathway (Lee, Park, Kim, Yoo, & Song, 2016; Sishi, Loos, van Rooyen, & Engelbrecht, 2013). Inhibition of the proteasome (25 nM and 50 nM PS-341) led to drastic increase in levels of wildtype Ank-B compared to control (Figure 3.4 A and B). Neither concentration of BafA affected wildtype Ank-B levels compared to control (Figure 3.4 A and B). These results suggested that wildtype Ank-B undergoes degradation by the proteasome.

I next hypothesized that p.S646FAnk-B protein levels could be rescued by proteasomal inhibition. Consistent with results of proteasomal inhibition on wildtype Ank-B (Figure 3.4 A and B), application of 10 nM PS-341 increased Ank-B expression for both wildtype and p.S646F above respective control levels (i.e. untreated wildtype or p.S646F transfected cells; Figure 3.4 C and D). Interestingly, 10 nM PS-341 treatment resulted in p.S646F-Ank-B levels comparable to those of untreated wildtype Ank-B control (Figure 3.4 C and D). These findings suggested that wildtype and p.S646F Ank-B were degraded via the proteasome, and inhibition of the proteasome rescued p.S646F Ank-B proteins levels.

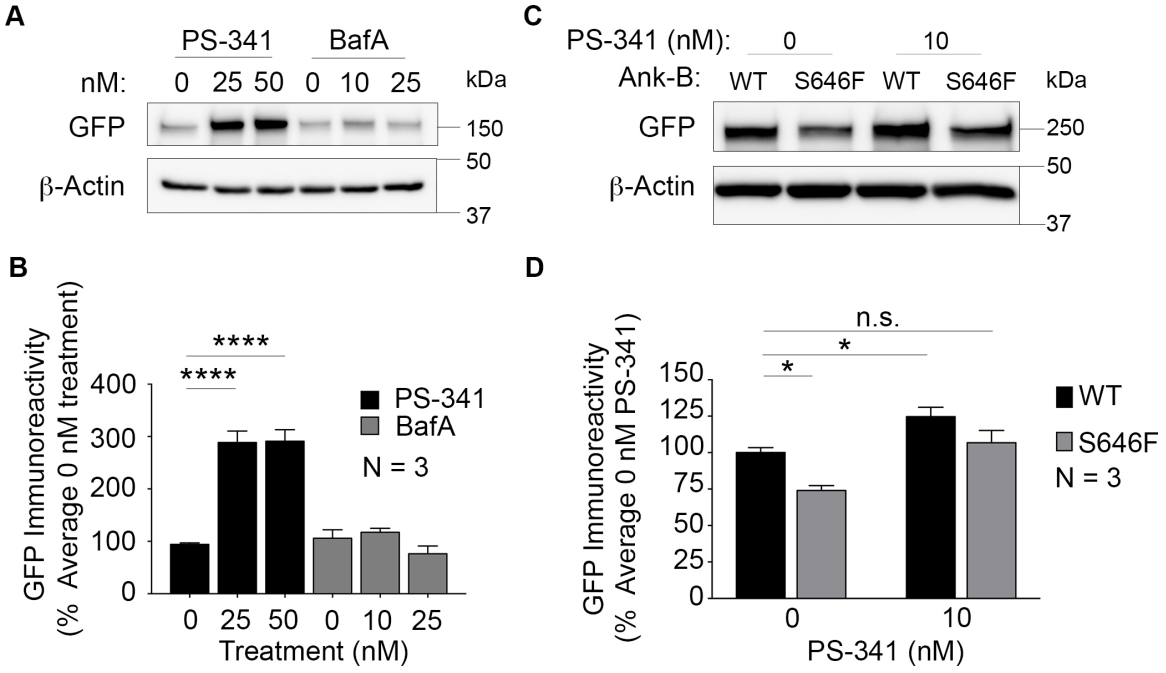

Figure 3.4 Ank-B is regulated by the proteasomal degradation pathway. A, Immunoblot of GFP-tagged wildtype-Ank-B from H9c2 lysates treated with 0 nM, 25 nM, and 50 nM proteasomal inhibitor, PS-341, or 0 nM, 10 nM and 25 nM lysosomal inhibitor, Bafilomycin A (BafA) 24 h post transfection, and collected 24 h post treatment. Immunoblots probed for anti-GFP (top) or anti-β-actin (bottom). **B,** Quantification of immunoblot revealed a significant increase in wildtype-Ank-B levels with PS-341 treatment and no differences with BafA treatment. All data was normalized to β-actin immunoreactivity and represented as % untreated control. ($P < 0.0001$ by one-way ANOVA, (****) $P < 0.0001$ by Dunnett's multiple comparison; N = 3). **C,** Immunoblot of H9c2 cells expressing GFP-tagged wildtype or p.S646F Ank-B treated with 0 nM or 10 nM PS-341 6 hours post-transfection. Cell lysates collected 12 h post PS-341 treatment were probed with anti-GFP (top) or anti–β-actin (bottom). **D,** Quantification of GFP immunoreactivity revealed a significant decrease in p.S646F-Ank-B 0 nM PS-341 compared to wildtype Ank-B 0 nM PS-341. Significant increase was observed with 10 nM PS-341 inhibition of wildtype Ank-B compared to 0 nM PS-341. p.S646F Ank-B levels were not significantly different from wildtype Ank-B control 0 nM PS-341 levels. All data was normalized to β-actin immunoreactivity and represented as % untreated

wildtype Ank-B expressing H9c2 (Genotype: $F(1,8) = 14.32$, $P = 0.0054$; Treatment: $F(1,8) = 24.48$, $P = 0.001$; Interaction: $F(1,8) = 0.4887$, $P = 0.5043$ by two-way ANOVA; Dunnett's multiple comparison (*) $P = 0.0326$ for wildtype 0 nM PS-341 and p.S646F 0 nMPS-341 (*), $P = 0.0416$ for wildtype 0nM PS-341 and wildtype 10nM PS-341, $P > 0.05$ for wildtype 0 nM PS-341 and p.S646F 10 nM PS-341; N=3).

3.3 Discussion

My work revealed that Ank-B p.S646F was less stable than the wildtype protein in H9c2 cardiomyoblasts. Furthermore, I found that Ank-B was degraded by the proteasome and that Ank-B p.S646F levels were rescued by proteasome inhibition. Here, I discuss the advantages and disadvantages to the methods used, and the relevance of these results in the context of Ank-B proteostasis.

My initial finding that mutant AnkB levels were significantly lower than wildtype AnkB levels 48 hours post-transfection suggested that the MBD could be important for Ank-B stability in the context of the cardiomyocyte/cardiomyoblast. HEK293T are a transformed epithelial-derived cell line (Thul et al., 2017; Uhlén et al., 2015); the equal expression levels observed in these cells suggests differences in expression levels of wildtype and mutant proteins is cell-type specific. In contrast to the relatively equal transfection efficiencies and expression levels in HEK293T cells, in H9c2 cells, expression levels of wildtype and mutant Ank-B were significantly different 48 hours post transfection. Additional work was conducted by our collaborators, Wang and Zhang, to determine whether the mutation affected the inherent stability of the pure MBD (Swayne et al., 2017). They performed a series of biochemical assessments on exclusively purified MBD of both wildtype and p.S646FAnk-B. Fast protein liquid

chromatography (FPLC) and circular dichromism (CD) methods were used to perform a structural comparison of the purified MBD of wildtype and mutant AnkB. No significant changes were observed in molecular weight or column behavior, nor helical structure and urea-induced denaturation dynamics. These findings further suggested the MBD of p.S646FAnk-B is properly synthesized and folded *in vitro.* Based on these data (and considering expression of the exogenous AnkB is under the control of the CMV promoter), it is reasonable to conclude that the differences in Ank-B protein expression observed in H9c2 cardiomyoblasts are due to post-translational mechanisms. For instance, p.S646F could alter intramolecular interactions between the MBD and other domains of Ank-B and/or change intermolecular interactions of Ank-B with other proteins.

To determine the rate of degradation of Ank-B, I attempted to perform CHX-mediated protein synthesis inhibition (Figure 3.3), which is routinely used for this purpose (Alvarez-Castelao et al., 2012). Despite its routine use, there are numerous caveats, most obviously the deleterious effects of protein synthesis inhibition on cell viability (that varies from cell line to cell line), especially for study of proteins with relatively long half-lives. My results suggest Ank-B has a long half-life, and therefore I was not able to observe full degradation of Ank-B prior to CHX-induced cell death. Moreover, a protein with a short half-life (and therefore reduced in expression by CHX) may be required to interact with Ank-B for Ank-B to be targeted for degradation. It is also important to note that translation arrest inhibits transcriptional machinery, possibly changing the transcription of proteins involved in Ank-B post translation modification and protein stability. Similarly, translation arrest can inhibit machinery involved in

degradation pathways, thereby potentially slowing the rate of Ank-B turnover. Another caveat is that proteins tagged at either the N- or C- terminus of the protein can differentially alter protein-protein interactions or post translational modifications, thus exhibiting different experimental half-lives. Furthermore, the robust CMV promoter (used in plasmid-driven expression of wildtype and mutant Ank-B) could compete with the ability of CHX to inhibit the plasmid-driven Ank-B expression. Indeed, peak synthesis levels were achieved for wildtype only at 18 h whereas p.S646F peaked at 6 h, thereby suggesting CHX inhibition was not effective at translational arrest until these time points. The results of CHX inhibition experiment suggest the mutant Ank-B was degraded slightly faster (Figure 3.3); however, additional approaches will be needed to confirm the half-life of Ank-B.

CHX proved to be an ineffective method of observing the rate of turnover for GFP-tagged plasmid-expressed Ank-B; however, application of similar strategies on models expressing levels of Ank-B more closely representing those of the endogenous protein may be more accurate than with overexpressing the GFP- tagged protein, as in my studies. Specifically, CRISPR-Cas9 technology could be used to can generate cells or mouse lines expressing p.S646F Ank-B expression at endogenous levels. In summary, CHX analysis of wildtype and p.S646F Ank-B confirmed a slight increase in mutant Ank-B degradation, but additional studies will be needed to validate this finding.

A complementary method of examining the regulation protein levels in the cell is via inhibition of protein degradation (Alvarez-Castelao et al., 2012). As previously described, cytosolic proteins are primarily targeted through the proteasomal degradation pathway, whereas integral membrane proteins are engulfed and degraded through the

lysosomal pathway. Ank-B, although technically a cytosolic protein, interacts with cytoskeletal elements such as β-spectrin via its SBD, and interacts highly with integral membrane proteins including channels and transporters via its MBD. PSD-95 and AKAPs, which similarly associate with membrane proteins and cytoskeleton in neuronal and cardiac cells respectively, are both regulated by the proteasomal degradation pathway. Considering similarity in the scaffolding roles of PSD-95 and AKAPS with Ank-B, in addition to similarities in close proximity to membranes, *I hypothesize that similar cell machinery and processes are recruited to regulate Ank-B*. Here I demonstrated that indeed, Ank-B is similarly degraded as other prominent scaffolding proteins, by the proteasome (Figure 3.4).

The proteasome inhibitor PS-341 is approved for human clinical use, particularly in cancer therapy (Teicher & Anderson, 2015). However, the effects are controversial as application of PS-341 may be therapeutic at certain concentrations but toxic at high doses (W. Li et al., 2015; Tuchman et al., 2017). In particular, cardiotoxicity was reported in rats upon treatment with PS-341, leading to cardiovascular dysfunction (Nowis et al., 2010). The specificity of PS-341-mediated inhibition of proteasome degradation to the protein of interest is limited as it affects the levels of all proteins; i.e. we cannot distinguish its effects on overexpressed Ank-B-GFP from its effects on native proteins that could regulate Ank-B-GFP levels. Furthermore, PS-341 may assist in increasing the quantity of p.S646F Ank-B, but whether the additional protein is functional is unknown .

How does the mutation lead to increased degradation by the proteasome? Protein Quality Control (PQC) is a series of processes by which cells maintain tight surveillance on proteins by controlling protein recycling and degradation (Buchberger et al., 2010).

PQC may be recruited and altered in response to changes in protein biochemistry, shifting proteostasis away from typical protein signaling and trafficking, and instead towards degradation (Buchberger et al., 2010). The folding of the pure MBD, which contains p.S646F, was normal in isolation, suggesting there was no inherent instability caused by the mutation within the MBD. However, the MBD has previously been shown to participate in intramolecular interactions with the CTD (Abdi et al., 2006). Mutations in Ank-B, including the p.S646F mutation studied here, may affect the three-dimensional structure in intramolecular interactions of the MBD with the CTD, or intermolecular interactions such as those with post translational modification machinery or other protein-protein interactions, all of which could reduce its stability, resulting in targeting for degradation. There are several examples of mutations leading to increased degradation; for example, a missense mutation in the gene encoding sarcoendoplasmic reticulum Ca^{2+}-ATPase leads to increased targeting for ubiquitination and degradation by the proteasome (Bianchini et al., 2014). It is possible the addition of the hydrophobic phenylalanine residue and resulting tertiary whole-protein structural changes increases the likelihood of p.S646F Ank-B ubiquitination and proteasome degradation (Hetz et al., 2011; Oikawa et al., 2012; Schröder & Kaufman, 2005).

Previously identified Ank-B mutants exhibited loss-of-function effects, characterized largely by changes in localization of associated ion channels and transporters (Mohler, Le Scouarnec, et al., 2007). Although the importance of these binding partners and their function in cells is apparent through changes in conductance, protein-binding, and co-localization associated with mutant expression (Mohler, Le Scouarnec, et al., 2007), these do not fully depict the potential importance of the Ank-B

protein in self-regulation of proteostasis. In Swayne et al., 2017, as with other Ank-B mutants (located outside of the MBD), changes in co-localization of binding partners were observed in immunolabelled primary cardiomyocyte cultures transfected with wildtype or p.S646F AnkB-GFP. However, non-MBD variants did not exhibit decreased protein levels (Mohler, Le Scouarnec, et al., 2007). It is reasonable to speculate the location of the p.S646F within the MBD rearranged the structure of Ank-B holoprotein to expose ubiquitination sites, uniquely recruiting additional degradation systems.

In summary, the novel findings of this Chapter show that p.S646F decreases Ank-B levels compared to wildtype, Ank-B was regulated by the proteasome and the p.S646F mutation slightly increased the rate of degradation. The levels of mutant Ank-B were rescued by proteasome inhibition with PS-341. This Chapter reveals the proteasome as the main system of Ank-B degradation, revealing potential molecular mechanisms underlying p.S646F Ank-B pathophysiology and a pathway to target for future therapy. It is still unknown if mitigation of p.S646F protein levels can recover Ank-B function, and how this p.S646F loss of function affects cellular behaviours. In Chapter 4, I investigate the role Ank-B plays in cardiomyocyte development, and how p.S646F modulates cardiomyocyte behaviour.

4 p.S646F Decreases Cell Viability

4.1 Overview

Having determined that p.S646F increased Ank-B degradation by the proteasome, I next investigated how expression of p.S646F affects cellular development. Changes in the expression levels of critical proteins often results in altered cellular behaviours. Previous reports have shown that reduced expression of Ank-B, or disease-associated mutations, resulted in changes in the expression levels and distribution of Ank-B binding-partners (Cornejo et al., 2013; Le Scouarnec et al., 2008; Mohler, Le Scouarnec, et al., 2007; Mohler et al., 2005). Loss-of-function of tripartite complex binding partners does not account for the heart structure-based pathologies associated with Ank-B. It is therefore likely that Ank-B plays additional cellular roles beyond that of excitation-contraction coupling. Considering the developmental deficits in Ank-B$^{+/-}$ mice and cardiomyopathies observed in the human population harbouring the p.S646F variant, perhaps the increased rate of Ank-B degradation facilitated by p.S646F influences viability and development of the cardiomyocyte. In this Chapter, I *hypothesize the p.S646F mutant changes cell behaviour.*

This Chapter, I first observed H9c2 cardiomyocyte growth in wildtype or p.S646F Ank-B transfected cells over-time to test my prediction that *the p.S646F mutant decreases cell viability.* My findings here demonstrated that p.S646F impacted H9c2 cell growth and viability. I then used an MTT assay detection to confirm changes in cell viability associated with p.S646F expression. I confirmed that p.S646F expression resulted in a slight but statistically significant reduction in cell viability. I also

investigated the expression of established differentiation markers in wildtype and mutant expressing H9c2. Cell expressing AnkB p.S646F-GFP exhibited altered levels of these markers compared with cells expressing wildtype AnkB-GFP. Together these results established a new role for Ank-B in cardiomyocyte development and revealed new molecular mechanisms underlying p.S646F pathophysiology.

4.2 Results

To determine the impact of p.S646F on cardiomyoblast growth, H9c2 cells were transfected with wildtype and mutant Ank-B and were counted every 24 h for 96 h in the presence of Trypan Blue (Figure 4.1). Trypan Blue is a large, negatively-charged diazo dye that enters cells only when the plasma membrane is compromised (Chan, Kuksin, Laverty, Saldi, & Qiu, 2015), allowing me to monitor dead (blue) and live (white) cells. There were significantly lower numbers of live cells in H9c2 cultures expressing p.S646F over time (Figure 4.1A).

In order to examine cell death, the percentage of dead cells in wildtype and p.S646F-expressing cultures was plotted over time (Figure 4.1 B). Indeed, p.S646F expression was associated with a significant (~19%) increase in the percentage of dead cells compared to wildtype at 6 h after plating (mutant: 41.3% ± 3.9; wildtype: 21.9% ± 3.9, $P < 0.0001$ Bonferonni's multiple comparison; Figure 4.1B). Therefore, p.S646F decreased H9c2 cell viability compared to wildtype during the initial lag phase. Interestingly, the calculated doubling times for wildtype and mutant-expressing cells were not significantly different (wildtype: 32.5 h , mutant: 30.3 h; $P = 0.5755$ by t-test, N = 5; Figure 4.1 A), suggesting the decreased live cell count over time was caused by the initial decrease in mutant-expressing cell viability during the lag phase.

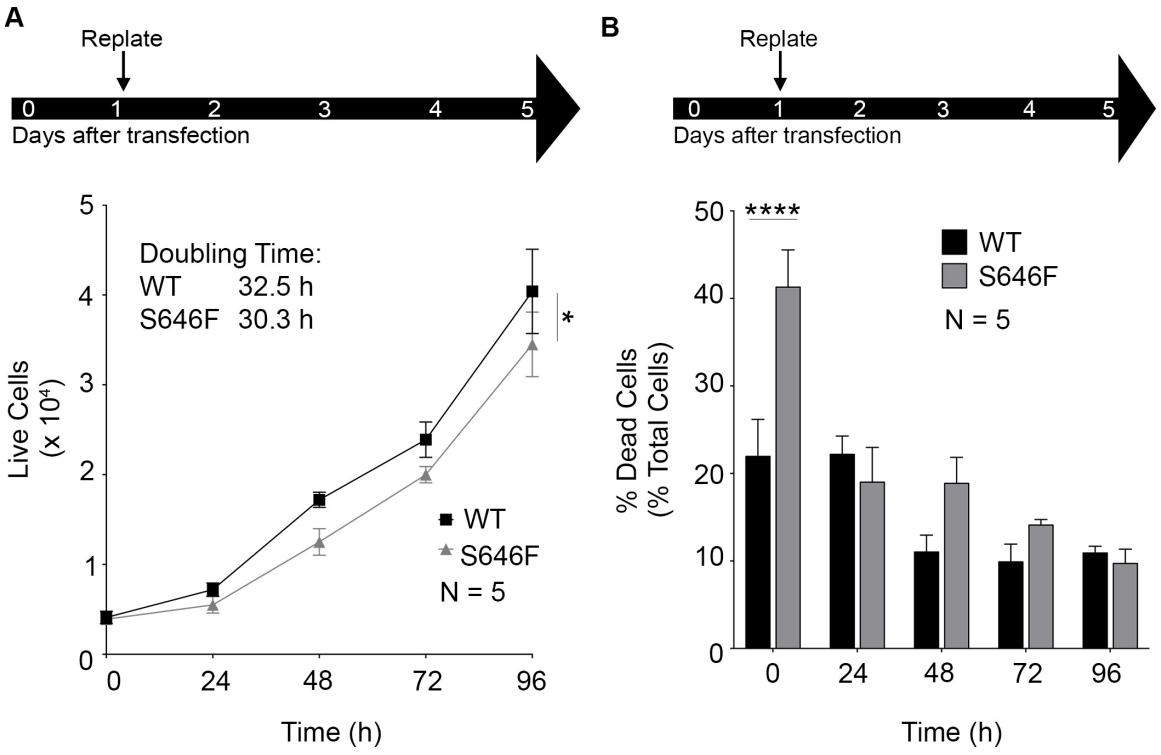

Figure 4.1 p.S646F decreased H9c2 cell viability. Cells were re-plated 24 h post-transfection. Live and dead cells were counted with Trypan Blue (0.4% Trypan Blue in PBS; Stem Cell Technologies) 6 h after re-plating ("0 h"), and every 24 h for 96 h. **A** Live cell numbers (x 10^4) across time. Doubling time for wildtype live cells and p.S646F live cells were 32.5 h and 30.3 h respectively. p.S646F transfected cultures exhibited significantly faster growth rate between 0 h and 96 h than wildtype (Genotype: $F(1,40) = 6.035$, $P = 0.0185$; Time: $F(4,40) = 81.86$, $P < 0.0001$; Interaction $F(4,40) = 0.5959$ $P = 0.6676$ by two-way ANOVA; Bonferroni's multiple comparisons indicate $P > 0.05$ between wildtype and p.S646F for all time points; N = 5). **B,** Dead cells, represented as a % total cell number for wildtype and p.S646F Ank-B cultures**.** (Genotype: $F(1,40) = 9.516$, $P = 0.0037$; Time: $F(4,40) = 19.33$, $P < 0.0001$, Interaction: $F(4,40) = 5.197$, $P = 0.0018$ by two-way ANOVA; Bonferroni's multiple comparison (****) $P < 0.0001$; N = 5).

MTT (tetrazolium salt (3-(4,5-Dimethylthiazol-2-yl)-3,5-diphenyltetrazolium bromide) assays were performed to determine mitochondrial activity (Figure 4.2). MTT is reduced to an insoluble formazan by mitochondrial dehydrogenase in living cells (Lax, Soler, & Fernández-Belda, 2006), shifting its absorption spectrum allowing for the measurement of mitochondrial function. A toxic dose (300 μg/mL) of CHX (Alvarez-Castelao et al., 2012), a protein translation inhibitor, served as a positive control for reduction in cell viability. H9c2 cells expressing p.S646F Ank-B-GFP exhibited ≈ 5% lower percentage of viable cells (p.S646f: 74.1% ± 2.6, wildtype 82.5% ± 2.6). These results confirmed p.S646F had a small but significant impact on H9c2 cell viability.

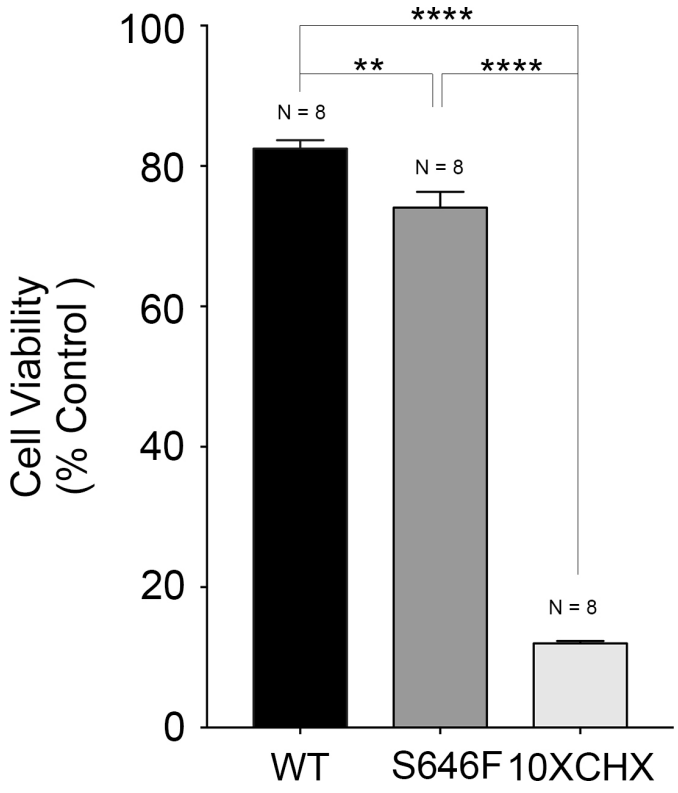

Figure 4.2 H9c2 expressing Ank-B p.S646F were slightly less viable than wildtype Ank-B expressing cells. MTT assay conducted 48 h post-transfection with wildtype or

p.S646FAnk2-GFP transfected H9c2. Toxic 300 μg/mL cycloheximide (10X CHX) treated cells were a positive control for reduced cell viability. All data was normalized to blanks (MTT solution in cell culture media alone), and presented as % untransfected control. ($P < 0.0001$ by one-way ANOVA, (**) $P = 0.0019$ and (****) $P < 0.0001$ by Bonferroni's multiple comparisons; N = 8).

Ank-B has previously been shown to impact the development of neonatal cardiomyocytes (Cunha et al., 2007). It is becoming increasingly accepted that cell death and differentiation share many common pathways (Bell & Megeney, 2017). Therefore I next investigated whether the deleterious effect of p.S646F on cell viability during the lag phase was associated with alteration of cellular differentiation signaling pathways. H9c2 cardiomyoblasts can be induced to differentiate with all-*trans* retinoic acid (RA) and reduced serum; thereby serving as a model for cardiomyoblast development (Branco et al., 2015). RA-differentiated H9c2 lysates were analyzed for levels of L-type calcium channel ($Ca_v1.2$), connexin 43 (Cx43), and cardiac troponin T (cTnT), by Western blotting (Figure 4.3). $Ca_v1.2$ prolongs depolarization, a characteristic feature of the cardiac action potential (Ménard et al., 1999), and has previously been shown to increase with H9c2 cell differentiation (Acosta et al., 2004). Cx43 is required for the formation of gap junctions and intercalated disc structure necessary for cell-cell communication required for the concerted contraction of cardiomyocyte (Song et al., 2010); and has previously been shown to decrease with RA-treatment of cardiomyocytes (Gu et al., 2016). Lastly, cardiac Troponin T (cTnT), is an essential protein required for the sarcomeric contractile structure of the mature cardiomyocytes (Branco et al., 2015; Sumi, Abe, & Himeno, 2013), and increases with cardiomyoblast differentiation (Branco et al., 2015). RA-treated H9c2 cells exhibited significant differences across time for all 3

markers. Specifically, $Ca_v1.2$ levels increased (Figure 4.3 B), Cx43 levels decreased (Figure 4.3 D), and cTnT levels increased (Figure 4.3 F) between 1 and 5 days of RA treatment. These trends in differentiation marker expression were consistent with previous studies of RA-differentiated H9c2 (Branco et al., 2015; Gu et al., 2016).Therefore, RA-differentiation of H9c2 served as an appropriate model to study cardiomyocyte development.

To determine if p.S646F affected cardiomyoblast differentiation pathways, lysates from H9c2 cells expressing wildtype or mutant Ank-B were also analyzed for $Ca_v1.2$, Cx43, and cTnT. I compared the relative expression of these differentiation markers in H9c2 expressing either wildtype or mutant Ank-B. H9c2 cells transfected with wildtype or mutant Ank-B plasmid expressed both $Ca_v1.2$ and Cx43 (Figure 4.3 C and E). Neither wildtype nor p.S646F expressing H9c2 lysates expressed cTnT (Figure 4.3). Additional exposures of blots incubated with highly sensitive chemiluminescent reagent West Femto (ThermoFisher Scientific) did not reveal any detectable levels of cTnT in wildtype or p.S646F lysates. Interestingly, p.S646F had significantly lower expression of both $Ca_v1.2$ and Cx43 at Day 1 (24 hours after transfection). Differences in wildtype or p.S646F Ank-B expressing culture were not present at later time points. In summary, compared to wildtype, mutant Ank-B transiently reduced differentiation marker levels, $Ca_v1.2$ and Cx43 suggesting p.S646F alters differentiation pathways in H9c2. The results of differentiation marker analysis are further discussed in the Discussion section of this chapter.

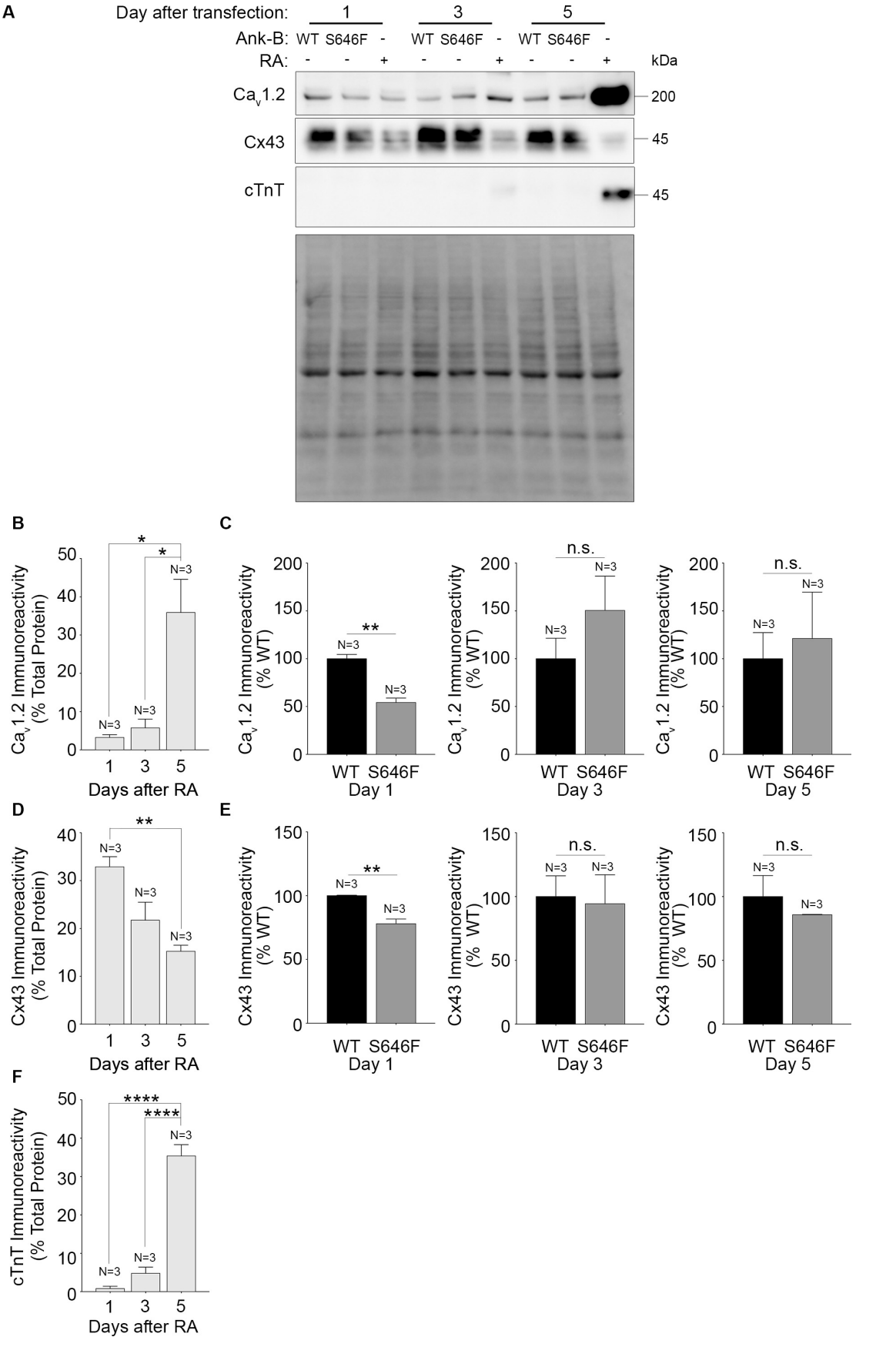
A
Day after transfection: 1 3 5
Ank-B: WT S646F - WT S646F - WT S646F -
RA: - - + - - + - - +
kDa
Cav1.2
200
Cx43
45
cTnT
45
B
Cav1.2 Immunoreactivity (% Total Protein)
Days after RA
C
Cav1.2 Immunoreactivity (% WT)
WT S646F
Day 1
Day 3
Day 5
n.s.
D
Cx43 Immunoreactivity (% Total Protein)
E
Cx43 Immunoreactivity (% WT)
F
cTnT Immunoreactivity (% Total Protein)
N=3

Figure 4.3Ank-B p.S646F mutations modulated expression of H9c2 differentiation markers. Immunoblot of H9c2 cell lysates collected 1, 3, or 5 days after transfection with wildtype or p.S646F-Ank-B-GFP plasmid, or treatment with low serum differentiation media (10 nM all-*trans* retinoic acid, 1% FBS). **A, Left,** Immunoblots probed for anti-$Ca_v1.2$ (top panel), anti-cTnT (second panel) or anti-Cx43 (third panel). Total protein stain (BioRad stainfree©) is shown on the bottom panel. **B,** $Ca_v1.2$ levels significantly increased in RA-treated cells over time, represented as % total protein (P = 0.0077 by one-way ANOVA, (*) P = 0.0104 for Day 1:Day5 and (*) P = 0.0151 for Day3:Day5 by Tukey's multiple comparisons; N = 3) **C,** $Ca_v1.2$ levels were significantly higher in wildtype cells at Day 1 ((**) P = 0.0021 by t-test; N = 3), but not at Day 3 or Day 5 (P = 0.2943 and P = 0.7250 respectively by t-test; N = 3). **D,** Cx43 immunoreactivity significantly decreased over time with RA treatment (P = 0.0083 by one-way ANOVA, (**) P = 0.0071 Day 1:Day3 by Tukey's multiple comparison; N = 3) **E,** Cx43 levels were significantly lower in p.S646F cultures at Day 1, ((**) P = 0.0041 by t-test; N = 3) but not at Day 3 or Day 5, N=3 (P = 0.8493 and P =0.4351 respectively by t-test; N =3). **F,** cTnT levels significantly increased in RA-treated cells over time (P < 0.0001 by one-way ANOVA; N =3, (****) P < 0.0001 Day Day 1:Day 5 and Day 3: Day 5; N = 3). No signal was detected for cTnT immunoreactivity in wildtype or p.S646F transfected cultures.

To detect overt structural differences in wildtype and mutant Ank-B expressing cells, we used confocal microscopy to observe phalloidin staining and examine actin striations and cell width/length (Figure 4.3). RA-differentiated cells exhibited a distinctly elongated morphology (consistent with cardiomyocyte differentiation). Wildtype and p.S646F exhibited similar actin striations to RA differentiated cells. A few elongated cells were observed in RA-differentiation conditions, while no elongated cells were

observed in Ank-B-expressing cells. No obvious differences in cell morphology were observed between wildtype and p.S646F expressing cells. These results are consistent with the subtle nature of the differences in differentiation marker expression observed by Western blotting. In future studies, we plan to quantify cellular AnkB levels and correlate these with metrics of cellular morphology and expression of differentiation markers.

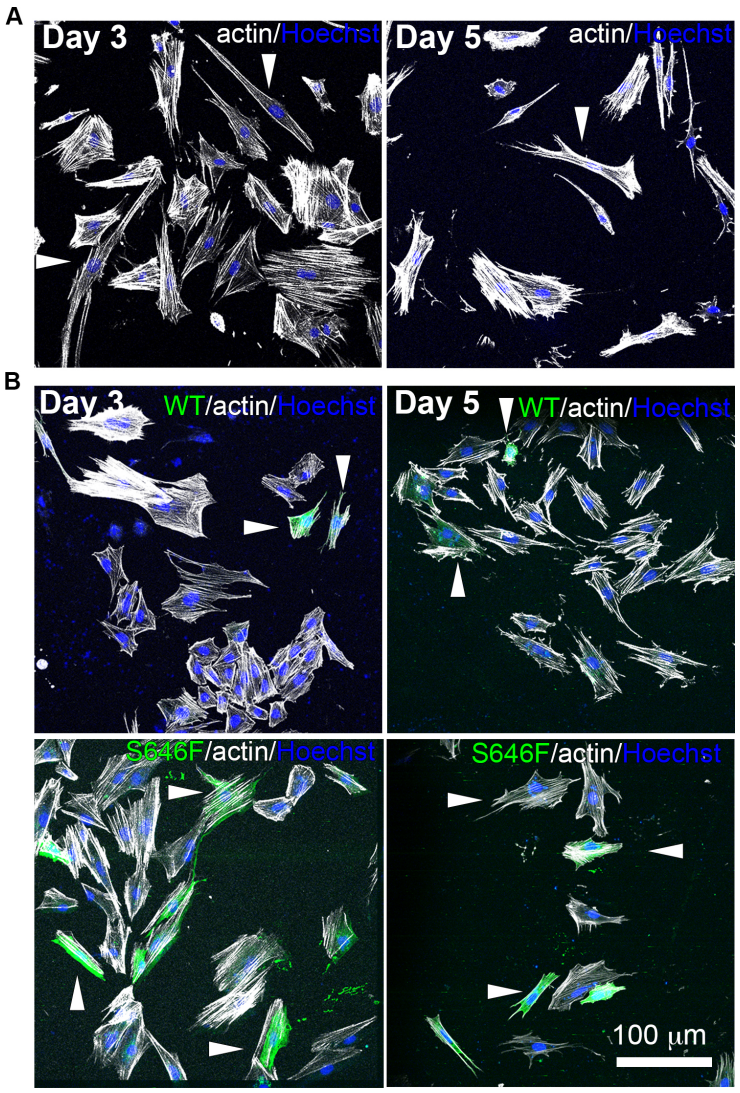

Figure 4.4 Ank-B expressing cells have similar physical features. H9c2 cells seeded onto PDL-laminin coated coverslips collected on Day 3 or Day 5 post-transfection or treatment, stained with Hoechst (blue) nuclear marker, and Phalloidin (white), an actin marker. White arrows indicate representative cells. **A,** H9c2 cells cultured in differentiation media (10 nM all-*trans* retinoic acid, 1% FBS) exhibited distinct elongation, a characteristic feature of cardiomyoblast differentiation and striated cytoskeletal staining. **B,** wildtype Ank-B-GFP or p.S646F-Ank-B-GFP plasmid transfected cells exhibited diffuse GFP expression (green) and actin-labeled striations (white) similar to differentiated H9c2 cells shown in A. White arrows indicate representative cells.

4.3 Discussion

This Chapter elucidated novel molecular mechanisms by which p.S646F impacts H9c2 cardiomyocyte cell behaviour. In this Chapter, I first assessed the live cell counts over time (Figure 4.1). Typically, the growth of cells exhibit a lag phase, an exponential growth phase, and then a plateau, varying in rate and duration of each phase depending on cell type (Kimes & Brandt, 1976; Suhaeri et al., 2015). Here, I demonstrated that wildtype Ank-B transfected H9c2 cells exhibited greater live cell counts, despite a similar doubling time (Figure 4.1). This difference in cell growth over time was likely due to an initial increase in cell death in p.S646F-expressing cells during the lag phase.

I compared the trends of differentiation marker between wildtype and mutant expression, with the trends observed with RA-differentiation H9c2 across 5 days. p.S646F transfected cultures expressed lower levels of $Ca_v1.2$ compared to wildtype on Day 1. In contrast, RA-differentiation of H9c2 decreased $Ca_v1.2$ levels across days, suggesting the mutant may be suppressing differentiation pathways. In contrast, p.S646F transfected cultures exhibit a lower expression of Cx43, which is consistent with the lowering of Cx43 expression in RA-differentiated H9c2 (Gu et al., 2016). Neither wildtype nor p.S646F Ank-B expressing cultures expressed cTnT. Together, these results suggest p.S646F alters differentiation pathways compared to wildtype. Future experiments should include quantification of relative abundance of other differentiation markers such as MHC, phospholamban, Bcl-2 or SERCA1 (Branco et al., 2015) to identify the role of wildtype and p.S646F Ank-B in cellular development.

Although the processes of cell death and cell differentiation are often considered separate cellular fates, they can and often occur simultaneously, or be triggered by one

another. More specifically, Ank-B could be inducing cell differentiation, as suggested by my differentiation marker analysis. The process of differentiation is known to induce cell death (Bell & Megeney, 2017). Notably, the timing of reduced $Ca_v1.2$ and Cx43 expression in p.S646F expressing cultures coincided with the decrease in Ank-B levels (Figure 3.1), the reduced cell number during the lag phase of H9c2 proliferation (Figure 4.1), and the decreased cell viability via MTT assay (Figure 4.3). This suggests cells expressing p.S646F Ank-B began to die at the same time they were exhibiting altering differentiation pathways. After this 48 hour post-transfection time frame, p.S646F-negative cells could be conferred a selective advantage and overtake the culture. This would explain the lack of significant differences in doubling time between wildtype and p.S646F cultures during the exponential growth phase (Figure 4.1), and lack of differences observed in differentiation markers at later time points (Figure 4.4). This raises the possibility that decreases in p.S646F levels compared with WT could be at the culture-dish rather than cellular level. In future work, we plan to quantify cellular AnkB levels (and localization), in wildtype and mutant-expressing cells, and correlate these levels (and localization) with metrics of cellular morphology and expression of differentiation/apoptosis markers to more fully elucidate the impact of mutant AnkB expression on cell differentiation and viability.

As previously described, Ank-B is a known scaffold for many ion channels and transporters. It has previously been shown that Ank-B interacts directly with $Ca_v1.3$ L-type channel in atrial myocytes through *in vitro* binding assays with the MBD (Cunha et al., 2011). Although Cunha et al. did not find an interaction between Ank-B with a $Ca_v1.2$, their binding assay was conducted in exclusively atrial cardiomyocytes with a

truncated section of $Ca_v1.2$. Choice of cell line is particularly important for the study of L-type Ca^{2+} channels, particularly because $Ca_v1.2$ is highly expressed in ventricular cardiomyocytes. Therefore, whether Ank-B directly interacts with $Ca_v1.2$ is still unknown. Here, I demonstrated that a mutation in Ank-B reduces $Ca_v1.2$ expression, suggesting Ank-B may play a role in regulating $Ca_v1.2$ protein levels. Previous studies have ascribed other proteins such as Ank-G and membrane scaffolding protein bridging integrator 1 (BIN1), not Ank-B, as key scaffolds required for Cx43 expression and gap junction/intercalated disc formation (Basheer & Shaw, 2016). Similar to the p.S646F phenotype in the patient population, dysregulation of $Ca_v1.2$ and Cx43 lead to arrhythmia and cardiac disease (Basheer & Shaw, 2016). Here, I demonstrated that $Ca_v1.2$ and Cx43 expression are differentially expressed in wildtype and mutant AnkB-expression cells, suggesting Ank-B could additionally scaffold these ion channels. Confocal imaging revealed no overt differences in wildtype and mutant Ank-B expressing H9c2 cells (Figure 4.3), but the overall size and elongation were not quantified. The lack of overt differences between wildtype and p.S646F expressing cultures was consistent with the subtle differences detected in differentiation marker expression. Future confocal microscopy experiments will determine relative expression and compartmentalization/localization of wildtype and mutant AnkB in relation to $Ca_v1.2$ and Cx43 in wildtype and p.S646F cultures. Furthermore, immunoprecipitation assays will be used to confirm if these ion channels are interacting partners of Ank-B and whether the strength of interaction is affected by the mutation. Similarly, if $Ca_v1.2$ and Cx43 prove to be novel Ank-B binding partners, cell-surface biotinylation will be used to determine the effects of wildtype and mutant AnkB on their surface localization.

The data presented in this chapter revealed that p.S646F reduces cell viability. However, as described earlier, decreased cell viability can be triggered by either cell-differentiation or by direct cell death signal transduction pathways. Although this chapter identified reduced cell viability through trypan blue and MTT assays (Figure 4.2 and 4.3), we did not identify the specific cell death pathway; activated cell apoptosis or necrotic cell death (Marunouchi & Tanonaka, 2015; Orogo & Gustafsson, 2013). Comparing protein abundance of cellular markers, such as activated caspase-3, or rapid increases in Reactive Oxygen Species (ROS) will help to understand the mechanism of cell death (Branco et al., 2015; Sumi et al., 2013). Western blot analysis of apoptosis relative pathways (ex. caspase-3 or PARP1 cleavage) will be used to further distinguish between wildtype and p.S646F cell viability (Lax et al., 2006).

In summary, the results of this Chapter confirmed my hypothesis that p.S646FAnk-B decreased cell viability in H9c2 cardiomyocytes. I demonstrated a significant difference in p.S646F-transfected H9c2 cell count over time compared to wildtype due to an initial significant reduction in viable cells, quantified by Trypan Blue and MTT Assay. Intriguingly, my results further revealed $Ca_v1.2$ and Cx43 as potential novel interacting partners of Ank-B, of which their expression is altered by the p.S646F mutant. These findings suggest p.S646F impacts on H9c2 differentiation and viability, thereby providing an additional molecular mechanism underlying Ank-B related disease and development of cardiomyopathy.

5 General Discussion

The findings of this thesis revealed novel molecular mechanisms underlying the regulation of Ank-B proteostasis and Ank-B-dependent cell behaviours. In this chapter, I have outlined my findings with respect to contributions and current understanding of the Ank-B protein and the molecular mechanisms underlying its role in the cell. I have further discussed the implications of my results and future directions to expand on my findings.

5.1 Ank-B proteostasis

The foundational concept of my work is defining the proteostasis of Ank-B. Proteostasis is required to maintain appropriate proteins levels, and therefore normal cell functions (Balch, Morimoto, Dillin, & Kelly, 2008; Díaz-Villanueva et al., 2015). This section will discuss my results in the context of synthesis and degradation of Ank-B. I will then discuss the details of Protein Quality Control (PQC) and how the cell may employ this process to rapidly respond to perturbations in the cell, such as the p.S646F mutation mutations, which may lead to misfolding or aggregation of the Ank-B protein.

5.1.1 Ank-B synthesis and degradation

When considering levels of a protein, the processes of how the cell builds and tears down the protein are the basic building blocks. In the cell, the way in which proteins are formed and then removed can be encompassed by the terms ‘synthesis’ and ‘degradation’. Chapter 3 introduced mechanisms by which the synthesis and degradation of Ank-B occur and are regulated by the MBD. Both the p.S646F and wildtype plasmid were transfected and synthesized equivalently in HEK293T cells, a low endogenous Ank-

B-expressing cell line (Thul et al., 2017). Furthermore, studies conducted by our collaborators, in Swayne et al. 2017, show that the Ank-B MBD is equal in structure between wildtype and p.S646F through a collection of biochemical assays. Specifically, *in vitro* FPLC column behavior and denaturation analysis indicated an equivalence in MBD synthesis for both wildtype and p.S646F. Additional mRNA quantitation experiments may confirm equal transcription of p.S646F and wildtype constructs. Methods may include northern blotting, in situ hybridization, or Real Time- Polymerase Chain Reaction (RT-PCR). Although all three approaches can provide relative and absolute quantitation of mRNA, northern blotting and in situ hybridization are limited in their ability to distinguish between mRNA of the same size. The degree of high sensitivity provided by RT-PCR makes this a promising method for confirming the absence of mutant mRNA splicing or degradation. Overall, both cell culture and biochemical analysis used in Chapter 3 suggested that differences observed in levels of wildtype and p.S646F Ank-B are due to cardiac cell-specific changes in post-translational stability, as opposed to differences in initial expression levels.

On the opposing end of a protein life-cycle, Ank-B degradation mechanisms were founded in Chapter 3. I showed, for the first time, that Ank-B degradation was mediated by the proteasome. In relation to wildtype, p.S646F enhanced Ank-B rate of degradation. An additional novel finding was that PS-341 proteasomal inhibition raised Ank-B p.S646F to wildtype control levels. Therefore, proteostasis of Ank-B is dysregulated by p.S646F, and the proteasome can be modulated to rescue levels Ank-B p.S646F. My thesis has evaluated both the synthesis and degradation of Ank-B, which contribute to the understanding of underlying molecular mechanisms of Ank-B creation and elimination in

the cell. For a fuller description of Ank-B regulation, future studies must take place to understand the processes that occur in between synthesis and degradation, such as post translational modifications, and how these processes contribute to Ank-B stability.

5.1.2 Protein quality control

The native three-dimensional conformation of a protein is crucial for its proper functioning in the cell. The cell has developed mechanisms to ensure the structure of proteins are correct and detect when a protein may be misfolded. The cell's adaptive unfolded protein response (UPR) activates in response to misfolded proteins imbalances, as previously described (Díaz-Villanueva et al., 2015; Hetz et al., 2015). For instance, chaperone proteins involved in the UPR are activated in response to changes in the native conformation of proteins to fold, target for re-folding, or target for degradation. Many chaperone proteins exist throughout the cell to mediate and monitor proper protein structure, such as HSP70 and HSP90. Please see Díaz-Villanueva et al. 2015 for further reading regarding protein folding and mechanisms of proteostasis. Inability to resolve the imbalance of increased stress on the secretory pathway, namely the ER, can cause not only protein loss of function but also activation of apoptosis leading to chronic disease (Díaz-Villanueva et al., 2015). Bianchini et al. located a missense mutation in the gene encoding SERCA1 protein, resulting in misfolding of the protein, destabilizing resting Ca^{2+} on the cellular level, manifesting as pseudomyotonia, a chronic disease of the skeletal muscle (2014). This is just one example of many in which the etiology of disease can be attributed to failure in the modulation of native protein structure and inability to compensate through the UPR/UPS.

5.1.3 p.S646F and the unfolded protein response

The tertiary structure of the entire Ank-B protein in comparison to that of the Ank-B p.S646F mutant has yet to be determined. Though synthesis and protein folding of the MBD portion of Ank-B were unaltered for p.S646F (Swayne et al., 2017), it is possible that the mutation affects interactions with and between other domains. This may be likely, as the mutation is a substitution from a small and polar amino acid, S (serine), to a larger and hydrophobic amino acid, F (phenylalanine), and could lead to exposure of hydrophobic regions of the protein. Exposure of hydrophobic regions can cause conformational changes to proteins decreasing their functional performance. It is possible that through the UPR, ER-Associated Degradation is initiated, flagging mutant Ank-B as a misfolded protein to be aggregated and/or degraded in the ER or cytosol and be targeted for degradation. Interestingly, imaging of primary cardiomyocytes by our collaborators in Swayne et al. suggested aggregation of the Ank-B-GFP and associated binding partners (2017). Furthermore, here I demonstrated that p.S646F Ank-B was indeed targeted for increased degradation, and Ank-B degradation is mediated by the ubiquitin-proteasome system. Future experiments should include confocal microscopy of Ank-B in conjunction with compartment-specific markers to identify where p.S646F Ank-B is accumulated and narrow the candidate chaperone systems within the UPR and PQC that are recruited.

5.1.4 p.S646F and the unfolded protein response across the human life-span

The changes in chaperone population throughout aging has become a growing field of research, as it underlies a fundamental change in the biochemistry of cells throughout the human life span (Brandvold & Morimoto, 2015). As we age, specific chaperone protein populations shift according to new cellular demands (Morimoto &

Cuervo, 2014). In terms of Ank-B, it is possible that p.S646F alters chaperone recruitment for recycling and refolding towards chaperones targeting Ank-B towards degradation (ex. E3 ubiquitin ligases). This is a potential cellular mechanism describing age-dependent the prolonged QTc and late onset cardiomyopathy of patients with the p.S646F mutation (Swayne et al., 2017).

Youth appears to be a protective factor in the population of p.S646F-positive patients, as younger p.S646F-positive individuals are less likely to have experienced episodes of LQTS4-related clinical features (Figure 1.6) (Swayne et al., 2017). With the exception of two patients born with structural abnormalities (TAPVR) and accessory electrical systems (WPW), onset of LQT associated phenotypes, and severity of clinical features are revealed or amplified as patients age. Prior to studies conducted in this thesis, limited information was available to describe the molecular mechanisms underlying the observed clinical features of p.S646F variant patients. The studies outlined in this thesis, in combination with Swayne et al. 2017, identified changes to p.S646F Ank-B post-translational stability that may be mediated through chaperone processes of the PQC. Future studies comparing chaperone activity between wildtype and p.S646F Ank-B may inform the increased prominence of disease-phenotype in many p.S646F-positive individuals over time.

5.2 Ank-B regulates cellular behaviours

Previous studies of scaffolding proteins were limited to the characterization of functions of the proteins with which they associate (Chudasama et al., 2008; Vondriska et al., 2004). This has provided a plethora of information regarding channel and transporter localization and function, and has thereby linked Ank-B, responsible for that localization,

to conduction disorders in the heart (Kline, Scott, Curran, Hund, & Mohler, 2014; Mohler, Davis, et al., 2004; Mohler, Rivolta, et al., 2004; Tuvia et al., 1999). Previous research regarding Ank-B variants has similarly focused on the loss-of-function of Ank-B protein-binding partners (Mohler, Healy, et al., 2007; Mohler, Le Scouarnec, et al., 2007) rather the loss-of-function or proteostasis of Ank-B itself. My thesis has revealed new information on Ank-B proteostasis and a novel role for Ank-B in cell functions such as viability, cardiomyocyte differentiation and heart development.

5.2.1 p.S646F and cellular conduction

The p.S646F mutation is associated with cardiac and neuronal conduction deficits (Swayne et al., 2017). We qualitatively identified a mislocalization of Ank-B in addition to mislocalization of a critical excitation-contraction protein, NCX1 (Swayne et al., 2017). Additional experiments quantifying the effects of the mutation on Ank-B and interacting protein localization are now warranted. Similarly, future experiments should investigate whether the mutation affects the relative strength of association of Ank-B binding partners, to help understand why localization might be impaired.

This thesis further indicated that variation in cellular conduction deficits for the p.S646F mutation was unique from other Ank-B variants in that it not only presented with prolonged QT interval, but was also associated with additional cardiac and neuronal electrical-system disorders including Wolf-Parkinson-White's Syndrome, and seizures. Interestingly, mutations in neuronal Ank-G have been linked to bipolar disorder, schizophrenia and epilepsy (for full review of Ank-G and neurological disorders, see Leussis et al., 2012). Considering Ank-B's critical role in neuronal axon-development and localization of ion channels, (Figure 1.3), variants in Ank-B could similarly lead to

developmental disruption, predisposing individuals to epilepsy. Overall, the severity and broadness of symptoms in the human population suggests a distinctly different pathogenesis and etiology for p.S646F variant of Ank-B in electrical behavior of both cardiomyocyte and neurons.

5.2.2 p.S646F and cell death

Amongst conduction-related cell behaviours, my studies showed p.S646F Ank-B reduced H9c2 cell number and viability (Figure 4.1 and 4.2). The mechanism of cell death (i.e. apoptosis versus necrosis) was not determined; however, apoptosis and necrosis are not mutually exclusive as both morphological and biochemical characterization do not demonstrate a complete separation of the two (Bell & Megeney, 2017; Takemura, Kanoh, Minatoguchi, & Fujiwara, 2013). For instance, both processes of apoptosis and necrosis implicate a decline in mitochondria function. Interestingly, through an MTT assay of cell viability (Figure 4.2), my results identified significant decreases in functional mitochondrial activity associated with the p.S646F mutation. The following section discusses how decreased mitochondrial function can activate both apoptosis and necrosis with respect to our understanding of the p.S646F Ank-B mutation cellular physiology.

MTT assays assess viability by evaluating mitochondrial function based on the standard activity of mitochondrial dehydrogenases in healthy cells. Intriguingly, abnormal mitochondrial activity is an indicator of both extrinsic apoptotic death receptor activation of cell apoptosis, and of necrosis (Orogo & Gustafsson, 2013). Apoptosis is a highly-regulated pathway activated by death receptor activation at the plasma membrane or by mitochondrial permeabilization. Necrosis, on the other hand, is not regulated as

apoptosis is, but is considered uncontrolled and results in mitochondrial swelling and/or rupture, followed by inflammation.

Mitochondrial stress due to p.S646F could be a result of changes in Ca^{2+} homeostasis (Mohler et al., 2003; Tuvia et al., 1999). The function of mitochondria is often described as an energy creation and storage compartment through processes such as the tricarboxylic acid (TCA) cycle. Mitochondria also serve as Ca^{2+} storage compartments, buffering cytosolic Ca^{2+} to protect the cell from Ca^{2+} toxicity. Interestingly, the TCA cycle is dependent on Ca^{2+}. Excessive influx of Ca^{2+}, induced by p.S646F disruption of Ca^{2+} homeostasis (Figure 1.10), could lead to mitochondrial opening of the mitochondrial Ca^{2+} uniporter in the inner mitochondrial membrane, overload of Ca^{2+} in the mitochondria, and activation of cell death pathways (Orogo & Gustafsson, 2013).

5.2.3 Ank-B and cellular development

Reduction in cell viability, as shown in Chapter 4, could have resulted not only from cell death, but also altered cell differentiation, as suggested by differentiation markers analysis. I revealed $Ca_v1.2$ and Cx43 to be potential interacting proteins for Ank-B that are also associated with differentiated cardiomyocytes (Figure 5.1). Changes to $Ca_v1.2$ and Cx43 expression have been linked to increased cytosolic Ca^{2+} and activation of apoptotic pathways (Basheer & Shaw, 2016), causing changes in cellular development that manifest as disease.

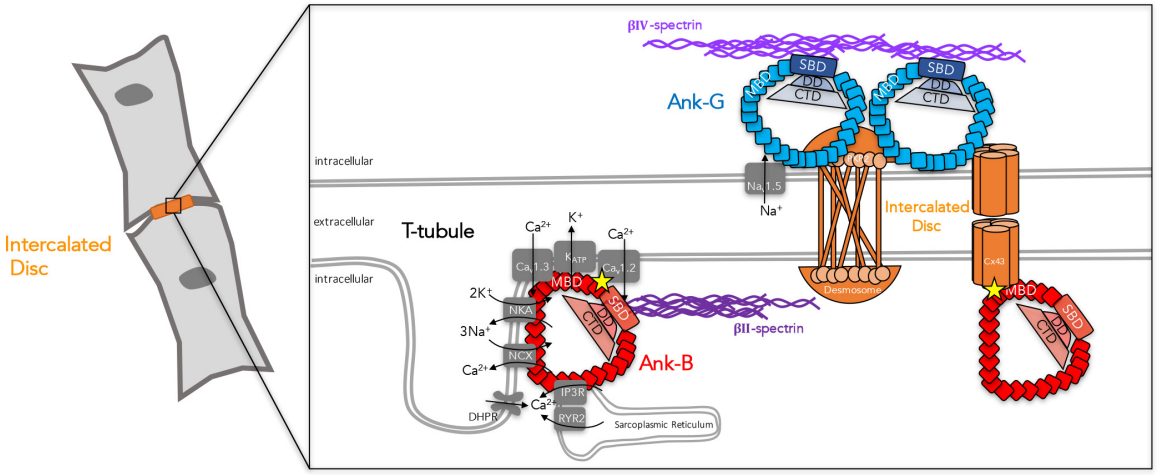

Figure 5.1 Ank-B and associated ion channels in the T-tubule and intercalated disc of the cardiomyocyte. Previous studies have demonstrated Ank-B's role in associating the tripartite complex necessary for T-tubule function and formation: NKA, NCX1, and IP3R. Additional studies have further identified K_{ATP}, and $Ca_v1.3$ bind to the MBD of Ank-B. My thesis revealed two new proteins that may interact with Ank-B in the T-tubule ($Ca_v1.2$, left yellow star), and gap junctions of the intercalated disc (Cx43, right yellow star).

As previously described, $Ca_v1.2$ and Cx43 are important for generation of the cardiac action potential, and the coordinated cell-cell communication required for synchronous cardiomyocyte contraction. Immunohistochemical analysis of L-type Ca^{2+} channel expression and Cx43 gap junctional protein expression in developing cardiomyoblasts has suggested regional and temporal expression of these proteins is critical for proper development and electrical properties of the heart (Acosta et al., 2004; Basheer & Shaw, 2016; van Kempen et al., 2003), in addition to development of the T-tubule and intercalated disc structures of the heart (Jenkins & Bennett, 2001; Jones & Svitkina, 2016). It is therefore reasonable to speculate that changes to Ank-B function and levels, which I have shown regulates these proteins, could alter differentiation.

Ank-B's potential role in development of cardiac and neuronal cells provides a molecular mechanism underlying the congenital cardiomyopathy and predisposition to seizures in the p.S646F patient population (Swayne et al., 2017). Although age is generally a protective factor reflecting possible changes in protective cell processes across the human life span, congenital structural abnormalities could be explained by p.S646F's role in modulating cell behaviours, propagating these cellular deficits in abnormal development of the whole-organ. In support of Ank-B's role in development, a vascular cardiomyopathy (Total Anomalous Pulmonary Vein Return) was associated with the p.S646F mutation (Swayne et al., 2017). Interestingly, neural crest stem cells give rise to not only the development of the neurons, but also the vasculature of the heart (Keyte & Hutson, 2012). Ablation of neural crest cells has been linked to abnormal valve and blood vessel formation or orientation (Keyte & Hutson, 2012). Further investigation is required to directly link Ank-B and its function in development across cell types.

5.3 Potential therapeutics

5.3.1 Current standard for Long QT Syndrome treatment

Due to the low frequency and relatively recent discovery of genetic link between Ank-B and LQTS4, the LQTS4 diagnosis and treatment remains niched within the current standard for all LQTS Types. The standard of method for investigation and treatment of LQTS consists of physical assessments by ECG, heart rate monitoring, and beta blockers (Drew et al., 2010). LQTS4 associated Ank-B variants differ from other LQTS types as their etiology does not arise from a single channelopathy, but rather a broad pathogenesis. Furthermore, we have shown the p.S646F mutant is associated with a syndrome comprised of unique symptoms compared to other Ank-B variants. In addition

to rhythm deficits associated with multiple ion channels, select p.S646F positive individuals also exhibit congenital and late onset structural cardiomyopathies, as well as neurological and vascular phenotypes. Therefore, management for general LQTS is likely inadequate for the LQTS4-affected individual, and particularly LQTS4-affected individuals harbouring the p.S646F variant. The molecular mechanisms unveiled by my thesis provide a backbone of knowledge for Ank-B protein regulation that can inform future targets for therapeutic research.

5.3.2 Proteasome inhibition

Proteasome inhibitors have been well researched in their efficacy for clinical treatment of disease, particularly cancer and stroke (Kisselev & Goldberg, 2001; Palumbo et al., 2016; Teicher & Anderson, 2015). A compilation of proteasome inhibitors have been shown to attenuate cardiac hypertrophy (N. Li et al., 2015) and cardiac fibrosis (Meiners et al., 2004), and has also been shown to restore the function of a mutant protein in cardiomyocytes (Azakir, Di Fulvio, Kinter, & Sinnreich, 2012) . Furthermore, proteasome inhibitors have been tested in neurons, showing the effect of proteasome inhibition is reversible and implicated in therapeutic potential for aging or age-related diseases (Ding, Dimayuga, Markesbery, & Keller, 2006). However, proteasome function is linked to widespread changes in mRNA expression, including heat shock protein chaperones that may beneficially buffer the levels and functional activity of Ank-B (Doll, Sarikas, Krajcik, & Zolk, 2007). Therefore, proteasome inhibitors must be carefully monitored in their dose and frequency while further investigations must outline their full effects on the whole proteome of cells.

PS-341, applied systemically, is the first proteasome inhibitor drug approved for clinical use. Its promise as a potential therapeutic was supported by my results (Figure 3.4). I showed the application of PS-341 was successful in increasing p.S646F Ank-B protein to wildtype control levels. However, ameliorating the total amount of p.S646F Ank-B protein may not be advantageous if the function of p.S646F is inadequate or deleterious in the cell. Therefore, additional mechanisms of enhancing the function and regulation of the p.S646F Ank-B protein must be considered.

5.3.3 Chaperone induction

Populations of chaperones fluctuate through our lifetime in any degree of proteostasis engagement. Induction of HSP70 and 90, the largest family of chaperone proteins, are shown to mitigate misfolded proteins, thereby assisting in restoring protein function (Brandvold & Morimoto, 2015). Alternatively, chemical chaperones are proven to be efficacious in the mitigation of UPR-related diseases (Cortez & Sim, 2014). For instance, hydrophobic chaperones such as 4-phenylbutyrate (4-PBA) attenuate ER stress in H9c2 cells (Chen, Liu, Chen, Zhang, & Gu, 2017). An important caveat of several chemical chaperone proteins is their narrow therapeutic dosage. This has been demonstrated with certain osmolytic chaperones, as they were effective only at high concentrations (Cortez & Sim, 2014; Winter et al., 2014). Nevertheless, molecular and chemical chaperone induction may serve as a viable option for improving the recycling, folding, and overall regulation of the p.S646F Ank-B protein.

5.4 Summary of thesis

Ank-B's function as a scaffolding protein has been well characterized in previous literature. My thesis used *in vitro* methods to identify novel pathways of Ank-B proteostasis and the effect of p.S646F on these processes. I elucidated the role of proteasome in Ank-B degradation and the effects of a novel Ank-B variant on cell viability and differentiation. The p.S646F mutation 1) decreased Ank-B protein expression, 2) increased rate of Ank-B degradation by the proteasome, 3) decreased cell viability and 4) altered the expression of differentiation markers. The data presented in this thesis represents the first characterization of the novel-disease causing Ank-B mutation, contributing to our understanding of the Ank-B protein and Ank-B-associated disease phenotypes.

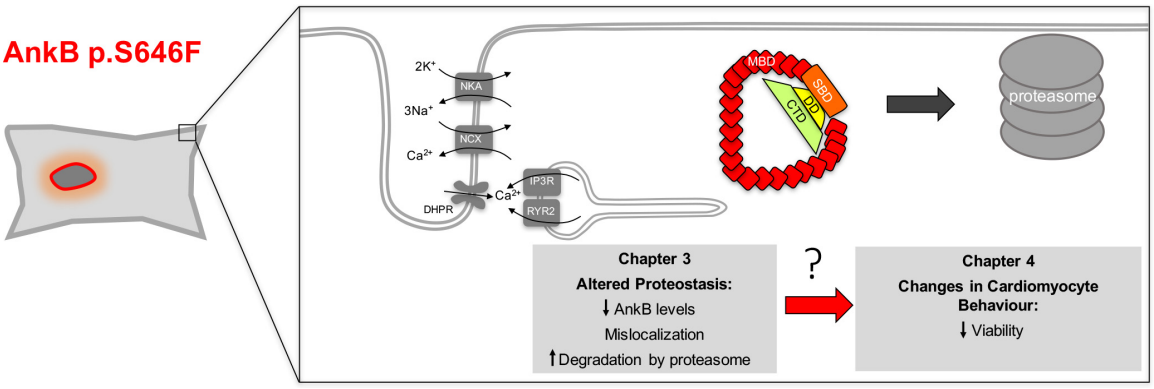

Figure 5.2 Summary of p.S646F effect on Ank-B proteostasis and cell behaviour. Chapter 3 described the decrease in p.S646F Ank-B levels cardiomyocytes, in part due to increased degradation by the proteasome. I showed, in Chapter 4, p.S646F reduced cell viability and modulated expression of differentiation markers. These findings demonstrated p.S646F altered Ank-B proteostasis, which in turn, through mechanisms to be studied in the future, altered cardiomyocyte behaviours.

6 References

Abdi, K. M., Mohler, P. J., Davis, J. Q., & Bennett, V. (2006). Isoform specificity of ankyrin-B: a site in the divergent C-terminal domain is required for intramolecular association. *Journal of Biological Chemistry*, *281*(9), 5741–5749. https://doi.org/10.1074/jbc.M506697200

Acosta, L., Haase, H., Morano, I., Moorman, A. F. M., & Franco, D. (2004). Regional expression of L-type calcium channel subunits during cardiac development. *Developmental Dynamics*, *230*(1), 131–136. https://doi.org/10.1002/dvdy.20023

Alders, M., Bikker, H., & Christiaans, I. (2018). Long QT Syndrome. In *GeneReviews®*. University of Washington, Seattle. Retrieved from http://www.ncbi.nlm.nih.gov/pubmed/20301308

Alvarez-Castelao, B., Ruiz-Rivas, C., & Castaño, J. G. (2012). A critical appraisal of quantitative studies of protein degradation in the framework of cellular proteostasis. *Biochemistry Research International*, *2012*, 823597. https://doi.org/10.1155/2012/823597

Arbour, L., Rezazadeh, S., Eldstrom, J., Weget-Simms, G., Rupps, R., Dyer, Z., … Fedida, D. (2008). A KCNQ1 V205M missense mutation causes a high rate of long QT syndrome in a First Nations community of northern British Columbia: a community-based approach to understanding the impact. *Genetics in Medicine : Official Journal of the American College of Medical Genetics*, *10*(7), 545–550. https://doi.org/10.1097/GIM.0b013e31817c6b19

Azakir, B. A., Di Fulvio, S., Kinter, J., & Sinnreich, M. (2012). Proteasomal inhibition restores biological function of mis-sense mutated dysferlin in patient-derived muscle cells. *Journal of Biological Chemistry*, *287*(13), 10344–10354. https://doi.org/10.1074/jbc.M111.329078

Balch, W. E., Morimoto, R. I., Dillin, A., & Kelly, J. W. (2008). Adapting proteostasis for disease intervention. *Science*, *319*(5865), 916–919. https://doi.org/10.1126/science.1141448

Basheer, W. A., & Shaw, R. M. (2016). Connexin 43 and CaV1.2 Ion Channel Trafficking in Healthy and Diseased Myocardium. *Circulation. Arrhythmia and Electrophysiology*, *9*(6), e001357. https://doi.org/10.1161/CIRCEP.115.001357

Bell, R. A. V, & Megeney, L. A. (2017). Evolution of caspase-mediated cell death and differentiation: twins separated at birth. *Cell Death and Differentiation*, *24*(8), 1359–1368. https://doi.org/10.1038/cdd.2017.37

Bennett, V., & Healy, J. (2008). Organizing the fluid membrane bilayer: diseases linked to spectrin and ankyrin. *Trends in Molecular Medicine*, *14*(1), 28–36. https://doi.org/10.1016/j.molmed.2007.11.005

Bennett, V., & Healy, J. (2009). Membrane domains based on ankyrin and spectrin associated with cell-cell interactions. *Cold Spring Harbor Perspectives in Biology*, *1*(6), 1–19. https://doi.org/10.1101/cshperspect.a003012

Bennett, V., & Stenbuck, P. J. (1979). Identification and partial purification of ankyrin , the high affinity membrane attachment site for human erythrocyte Identification Membrane and Partial Purification of Ankyrin , Attachment Site for Human Erythrocyte the High Affinity Spectrin *. *Journal of Biological Chemistry*, *254*(7), 2533–2541.

Bennett, V., & Stenbuck, P. J. (1979). The membrane attachment protein for spectrin is associated with band 3 in human erythrocyte membranes. *Nature*, *280*, 468–473. Retrieved from http://dx.doi.org/10.1038/280468a0

Bergmann, O., Bhardwaj, R. D., Bernard, S., Zdunek, S., Barnabé-Heider, F., Walsh, S., … Frisén, J. (2009). Evidence for cardiomyocyte renewal in humans. *Science*, *324*(5923), 98–102. https://doi.org/10.1126/science.1164680

Bianchini, E., Testoni, S., Gentile, A., Calì, T., Ottolini, D., Villa, A., … Sacchetto, R. (2014). Inhibition of Ubiquitin Proteasome System Rescues the Defective Sarco(endo)plasmic Reticulum Ca $^{2+}$ -ATPase (SERCA1) Protein Causing Chianina Cattle Pseudomyotonia. *Journal of Biological Chemistry*, *289*(48), 33073–33082. https://doi.org/10.1074/jbc.M114.576157

Branco, A. F., Pereira, S. P., Gonzalez, S., Gusev, O., Rizvanov, A. A., & Oliveira, P. J. (2015). Gene Expression Profiling of H9c2 Myoblast Differentiation towards a Cardiac-Like Phenotype. *PloS One*, *10*(6), e0129303. https://doi.org/10.1371/journal.pone.0129303

Brandvold, K. R., & Morimoto, R. I. (2015). The Chemical Biology of Molecular Chaperones--Implications for Modulation of Proteostasis. *Journal of Molecular Biology*, *427*(18), 2931–47. https://doi.org/10.1016/j.jmb.2015.05.010

Brette, F., & Orchard, C. (2003). T-tubule function in mammalian cardiac myocytes. *Circulation Research*, *92*(11), 1182–1192. https://doi.org/10.1161/01.RES.0000074908.17214.FD

Buchberger, A., Bukau, B., & Sommer, T. (2010). Protein Quality Control in the Cytosol and the Endoplasmic Reticulum: Brothers in Arms. *Molecular Cell*, *40*(2), 238–252. https://doi.org/10.1016/j.molcel.2010.10.001

Chan, L. L.-Y., Kuksin, D., Laverty, D. J., Saldi, S., & Qiu, J. (2015). Morphological observation and analysis using automated image cytometry for the comparison of trypan blue and fluorescence-based viability detection method. *Cytotechnology*, *67*(3), 461–73. https://doi.org/10.1007/s10616-014-9704-5

Chen, M., Liu, Q., Chen, L., Zhang, L., & Gu, E. (2017). Remifentanil postconditioning ameliorates histone H3 acetylation modification in H9c2 cardiomyoblasts after hypoxia/reoxygenation via attenuating endoplasmic reticulum stress. *Apoptosis*, *22*(5), 662–671. https://doi.org/10.1007/s10495-017-1347-5

Chudasama, N. L., Marx, S. O., & Steinberg, S. F. (2008). Scaffolding proteins in cardiac myocytes. *Handbook of Experimental Pharmacology*, *186*, 301–325. https://doi.org/10.1007/978-3-540-72843-6-13

Claycomb, W. C., Lanson, N. A., Stallworth, B. S., Egeland, D. B., Delcarpio, J. B., Bahinski, A., … Jr. (1998). HL-1 cells: a cardiac muscle cell line that contracts and retains phenotypic characteristics of the adult cardiomyocyte. *Proceedings of the National Academy of Sciences of the United States of America*, *95*(6), 2979–84. Retrieved from http://www.ncbi.nlm.nih.gov/pubmed/9501201

Cornejo, V. H., Pihán, P., Vidal, R. L., & Hetz, C. (2013). Role of the unfolded protein response in organ physiology: lessons from mouse models. *IUBMB Life*, *65*(12), 962–75. https://doi.org/10.1002/iub.1224

Cortez, L., & Sim, V. (2014). The therapeutic potential of chemical chaperones in protein folding diseases. *Prion*, *8*(2), 197–202. https://doi.org/10.4161/pri.28938

Cunha, S. R., Bhasin, N., & Mohler, P. J. (2007). Targeting and stability of Na/Ca

exchanger 1 in cardiomyocytes requires direct interaction with the membrane adaptor ankyrin-B. *Journal of Biological Chemistry*, *282*(7), 4875–4883. https://doi.org/10.1074/jbc.M607096200

Cunha, S. R., Hund, T. J., Hashemi, S., Voigt, N., Li, N., Koval, O., … Mohler, P. J. (2011). Defects in Ankyrin-Based membrane protein targeting pathways underlie atrial fibrillation. *Circulation*, *124*, 1212–1222. https://doi.org/10.1161/CIRCULATIONAHA.111.023986

Dambrot, C., Passier, R., Atsma, D., & Mummery, C. L. L. (2011). Cardiomyocyte differentiation of pluripotent stem cells and their use as cardiac disease models. *Biochemical Journal*, *434*(1), 25 LP-35. https://doi.org/10.1042/BJ20101707

Díaz-Villanueva, J. F., Díaz-Molina, R., & García-González, V. (2015). Protein Folding and Mechanisms of Proteostasis. *International Journal of Molecular Sciences*, *16*(8), 17193–230. https://doi.org/10.3390/ijms160817193

Ding, Q., Dimayuga, E., Markesbery, W. R., & Keller, J. N. (2006). Proteasome inhibition induces reversible impairments in protein synthesis. *The FASEB Journal*, *20*(8), 1055–1063. https://doi.org/10.1096/fj.05-5495com

Doll, D., Sarikas, A., Krajcik, R., & Zolk, O. (2007). Proteomic expression analysis of cardiomyocytes subjected to proteasome inhibition. *Biochemical and Biophysical Research Communications*, *353*(2), 436–442. https://doi.org/10.1016/j.bbrc.2006.12.039

Drew, B. J., Ackerman, M. J., Funk, M., Gibler, W. B., Kligfield, P., Menon, V., … Zareba, W. (2010). Prevention of Torsade de Pointes in Hospital Settings. *Circulation*, *121*(8). Retrieved from http://circ.ahajournals.org/content/121/8/1047.long

Foglia, M. J., & Poss, K. D. (2016). Building and re-building the heart by cardiomyocyte proliferation. *Development (Cambridge, England)*, *143*(5), 729–40. https://doi.org/10.1242/dev.132910

Gu, R., Xu, J., Lin, Y., Zhang, J., Wang, H., Sheng, W., … Huang, G. (2016). Liganded retinoic acid X receptor α represses connexin 43 through a potential retinoic acid response element in the promoter region. *Pediatric Research*, *80*(1), 159–168. https://doi.org/10.1038/pr.2016.47

Hashemi, S. M., Hund, T. J., & Mohler, P. J. (2009). Cardiac ankyrins in health and disease. *Journal of Molecular and Cellular Cardiology*, *47*(2), 203–9. https://doi.org/10.1016/j.yjmcc.2009.04.010

Hetz, C., Chevet, E., & Oakes, S. A. (2015). Proteostasis control by the unfolded protein response. *Nature Cell Biology*, *17*(7), 829–38. https://doi.org/10.1038/ncb3184

Hetz, C., Martinon, F., Rodriguez, D., & Glimcher, L. H. (2011). The unfolded protein response: integrating stress signals through the stress sensor IRE1α. *Physiological Reviews*, *91*(4), 1219–43. https://doi.org/10.1152/physrev.00001.2011

Jackson, H. A., Mcintosh, S., Whittome, B., Asuri, S., Casey, B., Kerr, C., … Arbour, L. T. (2014). LQTS in Northern BC: Homozygosity for KCNQ1 V205M presents with a more severe cardiac phenotype but with minimal impact on auditory function. *Clinical Genetics*, *86*(1), 85–90. https://doi.org/10.1111/cge.12235

Jackson, H., Huisman, L. L.-A. S., Saatani, S., Arbour, L. L., Santanai, S., & Arbour, L. L. (2011). Long QT Syndrome. *Canadian Medical Association Journal*, *183*(11), 1272–1275. https://doi.org/10.1503/cmaj.100138/-/DC1

Jaganjac, M., Matijevic, T., Cindric, M., Cipak, A., Mrakovcic, L., Gubisch, W., & Zarkovic, N. (2010). Induction of CMV-1 promoter by 4-hydroxy-2-nonenal in human embryonic kidney cells. *Acta Biochimica Polonica*, *57*(2), 179–183. Retrieved from http://www.actabp.pl/pdf/2_2010/179.pdf

Jenkins, S. M., & Bennett, V. (2001). Ankyrin-G coordinates assembly of the spectrin-based membrane skeleton, voltage-gated sodium channels, and L1 CAMs at Purkinje neuron initial segments. *The Journal of Cell Biology*, *155*(5), 739–46. https://doi.org/10.1083/jcb.200109026

Jones, S. L., & Svitkina, T. M. (2016). Axon Initial Segment Cytoskeleton: Architecture, Development, and Role in Neuron Polarity. *Neural Plasticity*, *2016*. https://doi.org/10.1155/2016/6808293

Kajstura, J., Urbanek, K., Perl, S., Hosoda, T., Zheng, H., Ogorek, B., … Anversa, P. (2010). Cardiomyogenesis in the Adult Human Heart. *Circulation Research*, *107*(2), 305–315. https://doi.org/10.1161/CIRCRESAHA.110.223024

Keyte, A., & Hutson, M. R. (2012). The neural crest in cardiac congenital anomalies. *Differentiation; Research in Biological Diversity*, *84*(1), 25–40. https://doi.org/10.1016/j.diff.2012.04.005

Kimes, B., & Brandt, B. (1976). Properties of a clonal muscle cell line from rat heart. *Experimental Cell Research*, *98*(2), 367–381. https://doi.org/10.1016/0014-4827(76)90447-X

Kisselev, A. F., & Goldberg, A. L. (2001). Proteasome inhibitors: from research tools to drug candidates. *Chemistry & Biology*, *8*(8), 739–58. Retrieved from http://www.ncbi.nlm.nih.gov/pubmed/11514224

Kline, C. F., Scott, J., Curran, J., Hund, T. J., & Mohler, P. J. (2014). Ankyrin-B regulates Cav2.1 and Cav2.2 channel expression and targeting. *Journal of Biological Chemistry*, *289*(8), 5285–5295. https://doi.org/10.1074/jbc.M113.523639

Koenig, S. N., & Mohler, P. J. (2017). The evolving role of ankyrin-B in cardiovascular disease. *Heart Rhythm*, *14*(12), 1884–1889. https://doi.org/10.1016/J.HRTHM.2017.07.032

Kuznetsov, A. V., Javadov, S., Sickinger, S., Frotschnig, S., & Grimm, M. (2015). H9c2 and HL-1 cells demonstrate distinct features of energy metabolism, mitochondrial function and sensitivity to hypoxia-reoxygenation. *Biochimica et Biophysica Acta (BBA) - Molecular Cell Research*, *1853*(2), 276–284. https://doi.org/https://doi.org/10.1016/j.bbamcr.2014.11.015

Lax, A., Soler, F., & Fernández-Belda, F. (2006). Cytoplasmic Ca2+ signals and cellular death by apoptosis in myocardiac H9c2 cells. *Biochimica et Biophysica Acta (BBA) - Molecular Cell Research*, *1763*(9), 937–947. https://doi.org/10.1016/J.BBAMCR.2006.05.009

Le Scouarnec, S., Bhasin, N., Vieyres, C., Hund, T. J., Cunha, S. R., Koval, O., … Mohler, P. J. (2008). Dysfunction in ankyrin-B-dependent ion channel and transporter targeting causes human sinus node disease. *Proceedings of the National Academy of Sciences of the United States of America*, *105*(40), 15617–22. https://doi.org/10.1073/pnas.0805500105

Lee, H., Park, J., Kim, E. E., Yoo, Y. S., & Song, E. J. (2016). Proteasome inhibitors attenuated cholesterol-induced cardiac hypertrophy in H9c2 cells, *49*(5), 270–275. https://doi.org/10.5483/BMBRep.2016.49.5.187

Leussis, M. P., Madison, J. M., Petryshen, T. L., Shen, K., Wei, L., Shaw, J., … Garrido, J. (2012). Ankyrin 3: genetic association with bipolar disorder and relevance to disease pathophysiology. *Biology of Mood & Anxiety Disorders*, *2*(1), 18. https://doi.org/10.1186/2045-5380-2-18

Li, J., Kline, C. F., Hund, T. J., Anderson, M. E., & Mohler, P. J. (2010). Ankyrin-B regulates Kir6.2 membrane expression and function in heart. *Journal of Biological Chemistry*, *285*(37), 28723–28730. https://doi.org/10.1074/jbc.M110.147868

Li, N., Wang, H.-X., Han, Q.-Y., Li, W.-J., Zhang, Y.-L., Du, J., … Li, H.-H. (2015). Activation of the cardiac proteasome promotes angiotension II-induced hypertrophy by down-regulation of ATRAP. *Journal of Molecular and Cellular Cardiology*, *79*, 303–314. https://doi.org/10.1016/j.yjmcc.2014.12.007

Li, W., Fu, J., Zhang, S., Zhao, J., Xie, N., & Cai, G. (2015). The proteasome inhibitor bortezomib induces testicular toxicity by upregulation of oxidative stress, AMP-activated protein kinase (AMPK) activation and deregulation of germ cell development in adult murine testis. *Toxicology and Applied Pharmacology*, *285*(2), 98–109. https://doi.org/10.1016/j.taap.2015.04.001

Marunouchi, T., & Tanonaka, K. (2015). Cell Death in the Cardiac Myocyte. *Biological & Pharmaceutical Bulletin*, *38*(8), 1094–1097. https://doi.org/10.1248/bpb.b15-00288

Meiners, S., Hocher, B., Weller, A., Laule, M., Stangl, V., Guenther, C., … Stangl, K. (2004). Downregulation of Matrix Metalloproteinases and Collagens and Suppression of Cardiac Fibrosis by Inhibition of the Proteasome. *Hypertension*, *44*(4), 471–477. https://doi.org/10.1161/01.HYP.0000142772.71367.65

Ménard, C., Pupier, S., Mornet, D., Kitzmann, M., Nargeot, J., Lory, P., … Lory, P. (1999). Modulation of L-type calcium channel expression during retinoic acid-induced differentiation of H9C2 cardiac cells. *Journal of Biological Chemistry*, *274*(0021–9258 SB–IM), 29063–29070. https://doi.org/10.1074/JBC.274.41.29063

Mikawa, T., & Fischman, D. A. (1992). Retroviral analysis of cardiac morphogenesis: discontinuous formation of coronary vessels. *Proceedings of the National Academy of Sciences of the United States of America*, *89*(20), 9504–8. https://doi.org/https://doi.org/10.1073/pnas.89.20.9504

Mohler, P. J., Davis, J. Q., & Bennett, V. (2005). Ankyrin-B coordinates the Na/K ATPase, Na/Ca exchanger, and InsP 3 receptor in a cardiac T-tubule/SR microdomain. *PLoS Biology*, *3*(12), 1–10. https://doi.org/10.1371/journal.pbio.0030423

Mohler, P. J., Davis, J. Q., Davis, L. H., Hoffman, J. a., Michaely, P., & Bennett, V. (2004). Inositol 1,4,5-Trisphosphate Receptor Localization and Stability in Neonatal Cardiomyocytes Requires Interaction with Ankyrin-B. *Journal of Biological Chemistry*, *279*(13), 12980–7. https://doi.org/10.1074/jbc.M313979200

Mohler, P. J., Gramolini, A. O., & Bennett, V. (2002). Ankyrins. *Journal of Cell Science*, *115*(8), 1565–1566. Retrieved from http://jcs.biologists.org/content/115/8/1565

Mohler, P. J., Healy, J. A., Xue, H., Puca, A. A., Kline, C. F., Allingham, R. R., … Bennett, V. (2007). Ankyrin-B syndrome: enhanced cardiac function balanced by risk of cardiac death and premature senescence. *PloS One*, *2*(10), e1051. https://doi.org/10.1371/journal.pone.0001051

Mohler, P. J., Le Scouarnec, S., Denjoy, I., Lowe, J. S., Guicheney, P., Caron, L., …

Roden, D. M. (2007). Defining the Cellular Phenotype of "Ankyrin-B Syndrome" Variants. *Circulation*, *115*(4). https://doi.org/10.1161/CIRCULATIONAHA.106.656512

Mohler, P. J., Rivolta, I., Napolitano, C., LeMaillet, G., Lambert, S., Priori, S. G., & Bennett, V. (2004). Nav1.5 E1053K mutation causing Brugada syndrome blocks binding to ankyrin-G and expression of Nav1.5 on the surface of cardiomyocytes. *Proceedings of the National Academy of Sciences of the United States of America*, *101*(50), 17533–8. https://doi.org/10.1073/pnas.0403711101

Mohler, P. J., Schott, J., Gramolini, A. O., Dilly, K. W., Guatimosim, S., William, H., … Bennett, V. (2003). Ankyrin-B mutation causes type 4 long-QT cardiac arrhythmia and sudden cardiac death. *Nature*, *421*, 1–6. https://doi.org/10.1038/nature01384.1.

Mohler, P. J., Splawski, I., Napolitano, C., Bottelli, G., Sharpe, L., Timothy, K., … Bennett, V. (2004). A cardiac arrhythmia syndrome caused by loss of ankyrin-B function. *Proceedings of the National Academy of Sciences of the United States of America*, *101*(24), 9137–9142. https://doi.org/10.1073/pnas.0402546101

Morimoto, R. I., & Cuervo, A. M. (2014). Proteostasis and the aging proteome in health and disease. *The Journals of Gerontology. Series A, Biological Sciences and Medical Sciences*, *69 Suppl 1*(Suppl 1), S33-8. https://doi.org/10.1093/gerona/glu049

Nowis, D., Maczewski, M., Mackiewicz, U., Kujawa, M., Ratajska, A., Wieckowski, M. R., … Golab, J. (2010). Cardiotoxicity of the anticancer therapeutic agent bortezomib. *The American Journal of Pathology*, *176*(6), 2658–68. https://doi.org/10.2353/ajpath.2010.090690

Oikawa, D., Kitamura, A., Kinjo, M., & Iwawaki, T. (2012). Direct association of unfolded proteins with mammalian ER stress sensor, IRE1β. *PloS One*, *7*(12), e51290. https://doi.org/10.1371/journal.pone.0051290

Orogo, A. M., & Gustafsson, Å. B. (2013). Cell death in the myocardium: my heart won't go on. *IUBMB Life*, *65*(8), 651–6. https://doi.org/10.1002/iub.1180

Palumbo, A., Chanan-Khan, A., Weisel, K., Nooka, A. K., Masszi, T., Beksac, M., … CASTOR Investigators. (2016). Daratumumab, Bortezomib, and Dexamethasone for Multiple Myeloma. *New England Journal of Medicine*, *375*(8), 754–766. https://doi.org/10.1056/NEJMoa1606038

Porrello, E. R., Mahmoud, A. I., Simpson, E., Hill, J. A., Richardson, J. A., Olson, E. N., & Sadek, H. A. (2011). Transient Regenerative Potential of the Neonatal Mouse Heart. *Science*, *331*(6020), 1078–1080. https://doi.org/10.1126/science.1200708

Qin, J. Y., Zhang, L., Clift, K. L., Hulur, I., Xiang, A. P., Ren, B.-Z., & Lahn, B. T. (2010). Systematic Comparison of Constitutive Promoters and the Doxycycline-Inducible Promoter. *PLoS ONE*, *5*(5), e10611. https://doi.org/10.1371/journal.pone.0010611

Robaei, D., Ford, T., & Ooi, S.-Y. (2015). Ankyrin-B syndrome: a case of sinus node dysfunction, atrial fibrillation and prolonged QT in a young adult. *Heart, Lung & Circulation*, *24*(2), e31-4. https://doi.org/10.1016/j.hlc.2014.09.013

Ron, D., & Walter, P. (2007). Signal integration in the endoplasmic reticulum unfolded protein response. *Nature Reviews. Molecular Cell Biology*, *8*(7), 519–29. https://doi.org/10.1038/nrm2199

Schott, J. J., Charpentier, F., Peltier, S., Foley, P., Drouin, E., Bouhour, J. B., … Pascal,

O. (1995). Mapping of a gene for long QT syndrome to chromosome 4q25-27. *American Journal of Human Genetics*, *57*(5), 1114–22. Retrieved from http://www.ncbi.nlm.nih.gov/pubmed/7485162

Schröder, M., & Kaufman, R. J. (2005). The mammalian unfolded protein response. *Annual Review of Biochemistry*, *74*, 739–89. https://doi.org/10.1146/annurev.biochem.73.011303.074134

Schwartz, P. J., Stramba-Badiale, M., Crotti, L., Pedrazzini, M., Besana, A., Bosi, G., … Spazzolini, C. (2009). Prevalence of the Congenital Long-QT Syndrome. *Circulation*, *120*(18), 1761–1767. https://doi.org/10.1161/CIRCULATIONAHA.109.863209

Scriven, D. R., Dan, P., & Moore, E. D. (2000). Distribution of proteins implicated in excitation-contraction coupling in rat ventricular myocytes. *Biophysical Journal*, *79*(5), 2682–91. https://doi.org/10.1016/S0006-3495(00)76506-4

Sishi, B. J. N., Loos, B., van Rooyen, J., & Engelbrecht, A.-M. (2013). Autophagy upregulation promotes survival and attenuates doxorubicin-induced cardiotoxicity. *Biochemical Pharmacology*, *85*(1), 124–34. https://doi.org/10.1016/j.bcp.2012.10.005

Song, D., Liu, X., Liu, R., Yang, L., Zuo, J., & Liu, W. (2010). Connexin 43 hemichannel regulates H9c2 cell proliferation by modulating intracellular ATP and [Ca2+]. *Acta Biochimica et Biophysica Sinica*, *42*(7), 472–482. https://doi.org/10.1093/abbs/gmq047

Suhaeri, M., Subbiah, R., Van, S. Y., Du, P., Kim, I. G., Lee, K., & Park, K. (2015). Cardiomyoblast (h9c2) differentiation on tunable extracellular matrix microenvironment. *Tissue Engineering. Part A*, *21*(11–12), 1940–51. https://doi.org/10.1089/ten.TEA.2014.0591

Sumi, D., Abe, K., & Himeno, S. (2013). Arsenite retards the cardiac differentiation of rat cardiac myoblast H9c2 cells. *Biochemical and Biophysical Research Communications*, *436*(2), 175–9. https://doi.org/10.1016/j.bbrc.2013.05.069

Swayne, L. A., Murphy, N. P., Asuri, S., Chen, L., Xu, X., McIntosh, S., … Arbour, L. T. (2017). Novel Variant in the ANK2 Membrane-Binding Domain Is Associated With Ankyrin-B Syndrome and Structural Heart Disease in a First Nations Population With a High Rate of Long QT Syndrome. *Circulation: Cardiovascular Genetics*, *10*(1), e001537. https://doi.org/10.1161/CIRCGENETICS.116.001537

Takemura, G., Kanoh, M., Minatoguchi, S., & Fujiwara, H. (2013). Cardiomyocyte apoptosis in the failing heart ? A critical review from definition and classification of cell death. *International Journal of Cardiology*, *167*(6), 2373–2386. https://doi.org/10.1016/j.ijcard.2013.01.163

Teicher, B. A., & Anderson, K. C. (2015). CCR 20th Anniversary Commentary: In the Beginning, There Was PS-341. *Clinical Cancer Research*, *21*(5), 939–941. https://doi.org/10.1158/1078-0432.CCR-14-2549

Thul, P. J., Åkesson, L., Wiking, M., Mahdessian, D., Geladaki, A., Ait Blal, H., … Lundberg, E. (2017). A subcellular map of the human proteome. *Science*, *356*(6340). Retrieved from http://science.sciencemag.org/content/356/6340/eaal3321

Tuchman, S. A., Moore, J. O., DeCastro, C. D., Li, Z., Sellars, E., Kang, Y., … Gasparetto, C. G. (2017). Phase II study of dose-attenuated bortezomib, cyclophosphamide and dexamethasone ("VCD-Lite") in very old or otherwise

toxicity-vulnerable adults with newly diagnosed multiple myeloma. *Journal of Geriatric Oncology*, *8*(3), 165–169. https://doi.org/10.1016/j.jgo.2017.02.004

Tuvia, S., Buhusi, M., Davis, L., Reedy, M., Bennet, V., Bennett, V., & Bennet, V. (1999). Ankyrin-B Is Required for Intracellular Sorting of Structurally Diverse Ca2+ Homeostasis Proteins. *The Journal of Cell Biology*, *147*(5), 995–1007. https://doi.org/10.1083/jcb.147.5.995

Uhlén, M., Fagerberg, L., Hallström, B. M., Lindskog, C., Oksvold, P., Mardinoglu, A., … Pontén, F. (2015). Tissue-based map of the human proteome. *Science*, *347*(6220). https://doi.org/1126/science.1260419.

van Kempen, M., van Ginneken, A., de Grijs, I., Mutsaers, N., Opthof, T., Jongsma, H., & van der Heyden, M. (2003). Expression of the electrophysiological system during murine embryonic stem cell cardiac differentiation. *Cellular Physiology and Biochemistry : International Journal of Experimental Cellular Physiology, Biochemistry, and Pharmacology*, *13*(5), 263–70. https://doi.org/10.1159/000074541

Vondriska, T. M., Pass, J. M., & Ping, P. (2004). Scaffold proteins and assembly of multiprotein signaling complexes. *Journal of Molecular and Cellular Cardiology*, *37*(2), 391–397. https://doi.org/10.1016/j.yjmcc.2004.04.021

Wang, M., & Kaufman, R. J. (2016). Protein misfolding in the endoplasmic reticulum as a conduit to human disease. *Nature*, *529*(7586), 326–335. https://doi.org/10.1038/nature17041

Wang, Z., & Hill, J. (2015). Protein Quality Control and Metabolism: Bidirectional Control in the Heart. *Cell Metabolism*, *21*(2), 215–226. https://doi.org/10.1016/j.cmet.2015.01.016

Watkins, S. J., Borthwick, G. M., & Arthur, H. M. (2011). The H9C2 cell line and primary neonatal cardiomyocyte cells show similar hypertrophic responses in vitro. *In Vitro Cellular & Developmental Biology - Animal*, *47*(2), 125–131. https://doi.org/10.1007/s11626-010-9368-1

Winter, L., Staszewska, I., Mihailovska, E., Fischer, I., Goldmann, W. H., Schröder, R., & Wiche, G. (2014). Chemical chaperone ameliorates pathological protein aggregation in plectin-deficient muscle. *The Journal of Clinical Investigation*, *124*(3), 1144–57. https://doi.org/10.1172/JCI71919

Witek, P., Korga, A., Burdan, F., Ostrowska, M., Nosowska, B., Iwan, M., & Dudka, J. (2016). The effect of a number of H9C2 rat cardiomyocytes passage on repeatability of cytotoxicity study results. *Cytotechnology*, *68*(6), 2407–2415. https://doi.org/10.1007/s10616-016-9957-2

Wolf, R. M., Glynn, P., Hashemi, S., Zarei, K., Mitchell, C. C., Anderson, M. E., … Hund, T. J. (2013). Atrial fibrillation and sinus node dysfunction in human ankyrin-B syndrome: a computational analysis. *American Journal of Physiology. Heart and Circulatory Physiology*, *304*(9), H1253-66. https://doi.org/10.1152/ajpheart.00734.2012

Yong, S., Tian, X., & Wang, Q. (2003). LongQT4 Gene: The “Missing” Ankyrin. *Mol Interv*, *3*(3), 131–136. https://doi.org/10.1017/CBO9781107415324.004